Coastal Engineering 65 (2012) 38–55

Contents lists available at SciVerse ScienceDirect

Coastal Engineering

journal homepage: www.elsevier.com/locate/coastaleng

# A Global Ocean Wave (GOW) calibrated reanalysis from 1948 onwards

B.G. Reguero, M. Menéndez, F.J. Méndez *, R. Mínguez, I.J. Losada

*Environmental Hydraulics Institute "IH Cantabria", Universidad de Cantabria E.T.S.I de Caminos, Canales y Puertos. Avda. de los Castros s/n, 39005, Santander, Spain*

ARTICLE INFO

*Article history:*
Received 14 June 2011
Received in revised form 2 March 2012
Accepted 5 March 2012
Available online 4 April 2012

*Keywords:*
Waves
Wave climate
Reanalysis
Validation
Calibration
Outliers

ABSTRACT

Wind wave reanalyses have become a valuable source of information for wave climate research and ocean and coastal applications over the last decade. Nowadays, wave reanalyses databases generated with third generation models provide useful wave climate information to complement, both in time and space, the instrumental measurements (buoys and alimetry observations). In this work, a new global wave reanalysis (GOW) from 1948 onwards is presented. GOW dataset is intended to be periodically updated and it is based on a calibration of a model hindcast with satellite altimetry data, after verification against historical data. The outliers due to tropical cyclones (not simulated due to insufficient resolution in the wind forcing) are identified and not taken into account in the process to correct the simulated wave heights with the altimeter data. The results are validated with satellite measurements in time and space. This new calibrated database represents appropriately the wave climate characteristics since 1948 and aims to be the longest and up-to-date wave dataset for global wave climate variability analysis as well as for many coastal engineering applications.



## 1. Introduction

Ocean surface gravity waves are the result of an important exchange of energy and momentum at the ocean–atmosphere interface. Waves propagate through the ocean basins transporting the accumulated energy obtained from the wind. During wave propagation, some energy is dissipated through different processes. The knowledge about how energy from winds transfers into the seas and how this energy propagates and dissipates is of great importance for the scientific community, since it allows understanding and modeling of wave fields. This modeling is of utmost importance for design purposes in offshore and coastal engineering. Furthermore, current research topics in ocean studies require long time series of wave climate with high spatial resolution at a global scale. Some examples of these research topics are the evaluation and study of wave energy resources, ocean dynamics variability, definition of operable conditions in shipping routes, maintenance and repair strategies for offshore constructions, extreme wave analysis, etc. Besides engineering, climate change also demands tools and data to define long-term variability of wave climate within different scenarios. Note that for all these research trends, global wave fields containing long time series of wave climate parameters are required.

Over the last decades, there has been an increasing interest in collecting wave climate information through instrumental devices such as buoys and satellite altimetry. Buoy measurements provide very accurate time series records but they are relatively short and are sparsely located in space, most of them in the Northern Hemisphere. In addition, they usually present interruptions due to disruptions on the normal use caused by buoy failure and maintenance activities. In contrast, satellite observations present a global coverage and also provide information with a high level of precision (±3 cm, Krogstad & Barstow, (1999)). However, this source of data is only available since 1992 and with a non-regular time resolution. Both sources of information, buoys and altimetry, do not configure a temporal and spatial homogeneous record of ocean wave climate variables for most of the purposes mentioned above. This issue has motivated an increasing interest in wind wave models, which allow obtaining spatially homogenous long-time series of wave climate parameters, i.e. Wave Reanalyses Databases (WRD). However, as it has been pointed out by several authors (Caires et al., 2004; Cavaleri & Sclavo, 2006), WRD are not quantitatively perfect, presenting several deficiencies with respect to instrumental data. Despite those shortcomings, WRD constitute an optimal way to accurately interpolate data both in time and space, even for those locations where no instrumental measurements exist (Weisse & Von Storch, 2010). Results are accurate enough to make them suitable, if carefully applied, to be used for coastal engineering purposes as well to assess long-term changes and trends.

The most advanced state-of-the-art wind wave models are the third generation wave models (Komen et al., 1994). Two of the most relevant and widely used within this group are the wave models WAM (Hasselman et al., 1998) and Wavewatch III (Tolman, 2002b, 2009; Tolman et al., 2002) (denoted as WW3 in the following). Both models are recommended to be used for open ocean wave simulation

* Corresponding author.
*E-mail address:* gonzalezrb@unican.es (F.J. Méndez).

0378-3839/$ – see front matter © 2012 Elsevier B.V. All rights reserved.
doi:10.1016/j.coastaleng.2012.03.003

because non-linear and wave-bottom interactions are not appropriately addressed. For this reason, wave climate in coastal and shallow waters is poorly described with these models. For details about models focused on coastal and shallow waters conditions see Booij et al., (1999); Schneggenburger et al., (1997) or Camus et al., (2011).

Wind wave models are driven by wind fields and constrained by ocean sea/ocean cover. The quality of any WRD depends upon the quality of wind forcing (Feng et al., 2006). There are several global meteorological reanalysis carried out at different research centers and institutes. A comprehensive list, including their characteristics, can be found in Weisse & Von Storch, (2010). It is worth noting the following among them:

1. The ERA-40 project (Uppala et al., 2005), carried out by the European Center for Medium Range Weather Forecast (ECMWF), which also includes the computation of the wave fields (Sterl & Caires, 2005);
2. The NCEP/NCAR reanalysis project (Kalnay et al., 1996), which constitutes the longest and most up-to-date global reanalysis;
3. The Japan Meteorological Agency reanalysis, JRA-25 (Onogi et al., 2007), covering the period 1979 to 2004, which is specially focused on the study of tropical storms.
4. Recently, the ECMWF have developed a new reanalysis to replace the ERA-40. It covers the period from 1989 onwards (Dee et al., 2011) and it also includes wave computation.

Based on wind wave models and global meteorological reanalysis, many efforts have been made in the last decades to generate consistent sets of data to define the wave climatology. Sterl et al., (1998) computed the first ocean wave field using the ERA-15 surface winds. The success of this reanalysis led to couple a wave model to the ERA-40 wind reanalysis (Uppala et al., 2005) with a resolution of 1.5°×1.5° (latitude×longitude). In an independent study, these wind fields were used to force the ODG2P wave model for 1988 (ERA-40/ODGP2). Due to deficiencies of the ERA-40 wave dataset, results present certain overestimation of low wave heights and a considerable underestimation of large wave heights (see Sterl & Caires, (2005)). Caires & Sterl, (2005a) produced a corrected version of the dataset, named as C-ERA-40 with a significant improvement in the diagnostic statistics (Caires & Sterl, 2005b). They use a non-parametric correction method based upon non-parametric regression techniques. However, the corrected dataset still shows some underestimation of high quantiles. Based on NCEP/NCAR winds (1.25°×2.5°), global wave fields were obtained by Cox & Swail, (2001) for the period 1958–1997 using the ODGP2 wave model with resolution of 1.25°×2.5° (CS01). Motivated by deficiencies in the NCEP/NCAR input wind fields, Swail & Cox, (2000) carried out an intensive kinematic reanalysis of these winds in the North Atlantic using a finer wave model grid (0.62°×0.833°). Pacific Weather Analysis (Graham & Diaz, 2001) produced a 50-yr wave reanalysis (PWA-R) using NCEP/NCAR winds and the model WW3 on a 1°×1.5° grid for the North Pacific Ocean during the winter season. One of the first but prominent attempts to reconstruct past wave climate in the North-East Atlantic was carried out by the WASA group (WasaGroup, 1998). Later on, within the project HIPOCAS, a high resolution wave (and sea level) reanalysis (Pilar et al., 2008) was developed using the wave model WAM. More recently Dodet et al., (2010) computed a reanalysis with WW3 for the last six decades to analyze wave climate variability in the North-East Atlantic. It is worth noting that the temporal resolution of results vary between reanalyses, from 1 to 6 h. Caires et al., (2004) present a comparative study between some of the most relevant global WRD.

Changes over time in data sources, advances in data analysis techniques and evolution of the wind wave models have conducted to inhomegeneities between the wave results of the different reanalyses described above.

Therefore, available numerical data of wave climate vary both in time range and in quality. The aim of this paper is to present a new WRD with the following characteristics:

1. It pretends to be continuously updated, constituting a valuable dataset of wave climate parameters for engineering applications.
2. Global coverage.
3. Long length of the simulated records (time series of different wave statistical parameters and energy spectra from 1948 onwards).
4. High temporal resolution of the outputs (hourly).
5. Exhaustive validation using instrumental measurements from buoys and satellite altimetry.
6. Post-process using altimetry observations consisting of: (a) identification of possible outliers (from 1992) related to hurricanes and typhoons not appropriately reproduced by the numerical modeling, and (b) calibration of the model hindcast results to obtain a more accurate description of the wave statistical distribution according to instrumental data.

The rest of the manuscript is organized as follows. Section 2 presents the methodology to obtain the Global Ocean Waves (GOW) reanalysis. It also describes the instrumental wave data used for corrections and validation, the model description, and a preliminary validation of the results with instrumental data from buoy and altimeter observations. Correction procedures (outliers removal and calibration of wave heights) are also addressed in this section. Results and verification of the correction procedure are presented in Section 3. Finally, concluding remarks are outlined in Section 4.

## 2. Methodology

### 2.1. Introduction

The development of the GOW database encompasses several stages, which are summarized in the flow chart of Fig. 1. This study presents a calibration of a model hindcast with satellite wave height data, after verification against historical data. Firstly, the wave generation is obtained by using the WW3 model and the NCEP/NCAR global wind and ice cover datasets. In order to check the performance of the wave generation model and the quality of the forcing fields, a preliminary validation is done using both buoy and satellite altimetry data as benchmarks. Next stage consists of the calibration of the numerical

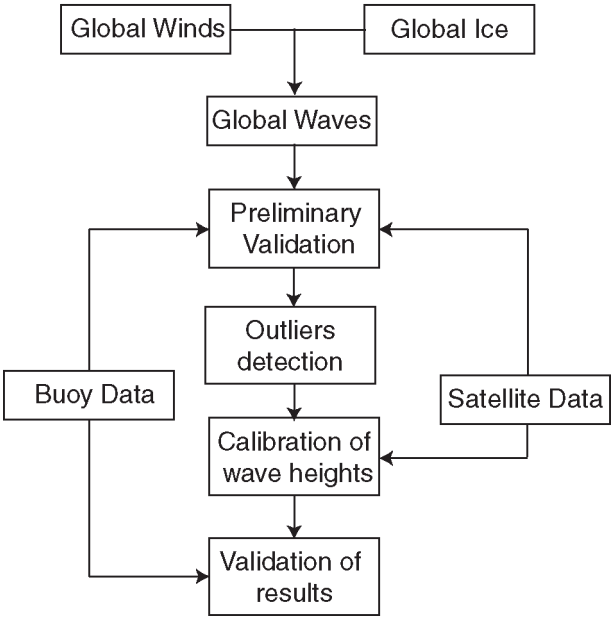


**Fig. 1.** Methodology diagram.

results (i.e. significant wave height) using satellite altimetry data. This process aims to make several systematic corrections to reduce deviations between the probability distribution function of corrected hindcast and instrumental data. However, previous to these corrections, an outlier detection process over the data pairs, both numerical and instrumental, is addressed. This filtering process is important to eliminate data related to hurricanes or typhoons episodes, which may be captured by the altimetry but are not appropriately reproduced in the forcing wind fields because of insufficient resolution. Finally, an additional validation using buoy data is carried out to check the performance of the calibration process and the quality of the final database. Hereafter, we will refer to the hindcast data as the Non-calibrated GOW (NC-GOW) results and we will use GOW for the results after applying the corrections.

### 2.2. Model set-up

The generation and propagation of the wind waves are simulated with the model WW3, version 2.22 (Tolman, 2002a). Simulations are computed on a global grid with a spatial resolution of 1.5° in longitude and 1° in latitude (a total of 22.945 computational nodes). Wave growth uses source terms (Tolman & Chalikov, (1996)) to account for wind input, non-linear wave-wave interactions and whitecapping. Effects of depth-induced refraction are also considered in the propagation model. Wave interactions with currents and island shadowing are not considered in the simulation process. Bathymetry data used for the simulation comes from the ETOPO dataset (NOAA, 2006). The minimum propagation time-step used for the computation was 60 s and the spectral resolution covers 72 regularly spaced directions. Frequencies extend from 0.03679 hz with 25 frequency steps and a frequency increment factor of 1.1.

Because wave model output is very sensitive to the wind field input choice, different studies have been developed to judge the quality of the wind fields. Tolman, (2002b) determines that the NCEP/NCAR winds provide the best results in terms of significant wave height estimates for the model WW3. More recently, Feng et al., (2006) analyze four different wind forcing fields with the WW3 model: (1) NCEP/NCAR reanalysis winds, (2) the ECMWF wind fields, (3) the QuickSCAT wind observations blending the NCEP/NCAR reanalysis winds and, finally, (4) an enhanced ECMWF wind field with assimilation of wind speed measurements. Their results indicate that NCEP/NCAR winds as input data produce the best agreement with TOPEX altimetry wave measurements, at both global and regional scales, while the others present a higher spatial variability and are all positively biased.

The long temporal coverage, the up-to-date characteristic, the continuously assimilated observations and the good evaluation obtained in the mentioned works, indicate that NCEP/NCAR wind fields are an adequate choice for wave modeling performance. Although data assimilation on NCEP/NCAR is maintained, special caution must be taken for the study of long-term changes due to the evolution of assimilated observations (Kistler et al., 1999). Inhomogeneities caused by changes in the amount of assimilated observations within NCEP-NCAR reanalysis are particularly relevant in the Southern Hemisphere and before 1980 (Sterl, 2004). Potential users must be aware of this fact and the use of the data in some regions of the Southern Hemisphere must be done with caution due to homogeneity problems (Sterl & Caires, 2005). Therefore, we force WW3 model with 6-hourly wind fields from the NCEP/NCAR Reanalysis project (Kalnay et al., 1996), available from 1948 to present. Wind data are defined on a Gaussian grid with a spatial resolution of approximately 1.9° in latitude and 1.875° in longitude. Simulations also include ice coverage fields from NCEP/NCAR.

The output parameters obtained all over the grid are: the significant wave height ($H_s$), mean wave period ($T_m$), peak period ($T_p$), peak direction ($\theta_p$), mean wave direction ($\theta_m$), directional spread and energy spectra in specific locations along the coast to analyze multimodal sea states, with different swell and wind sea components. This increment of data storage in coastal areas allow summing higher resolution wave propagation models (Camus et al., 2011) for engineering applications (ports, breakwaters, sediment transport, etc.). In this work we do not analyze the different swell and wind sea components as in Semedo et al., (2011), although they could also be obtained.

### 2.3. Validation data

An important aspect within WRD design is the validation process using instrumental information as a benchmark. For this particular issue, we compare wave model results with measurements from deep-water buoys at different locations over the Atlantic and Pacific oceans and the Caribbean Sea. In-situ buoy measured wave data are obtained from three different sources: NOAA National Data Buoy Center, the Environment Canada and Puertos del Estado (Spain). Table 1 includes the locations of the buoys used in the validation process, which are also represented in Fig. 6.

Although buoy observations are considered the most reliable wave measurements, they are scattered in time and space, mainly located in the Northern Hemisphere and are generally available for the last two decades. In contrast, altimetry wave measurements provide the best possible spatial coverage to evaluate global wave data. From the nineties, different satellite missions, such as, Jason 1, Jason 2, TOPEX, ERS-2, Envisat and GFO, incorporate altimetry sensors. Wave data from these sources show very good agreement between each other and, as a consequence, they are combined for comparison with reanalysis results. In this study, we have used the significant wave heights from the mentioned six satellite missions from 1992 to 2008. The calibration procedures summarized in Cotton, (1998) and Woolf & Challenor, (2002), and later updated by Hemer et al., (2010) using extra years and additional satellite missions have been applied to the altimeter measurements.

### 2.4. Preliminary validation

In order to assess the quality of the numerical simulated results, these are compared with respect to buoy and altimetry data. Different wave parameters ($H_s$, $T_p$ and $\theta_m$) are compared in a total of 21 buoy stations, some of them directional gauges. Several diagnostic statistics for comparing model performance ($y$) with respect to instrumental data ($x$) are calculated:

- The systematic deviation between two random variables (BIAS; usually model minus data):

$$\mathrm{BIAS} = \bar{x} - \bar{y}. \tag{1}$$

- The root mean square error (RMSE):

$$\mathrm{RMSE} = \sqrt{\frac{1}{n_d}\sum_{i=1}^{n_d}(x_i - y_i)^2}. \tag{2}$$

- The residual scatter index (SI), which measures dispersion with respect to the line $x = y$:

$$\mathrm{SI} = \frac{\mathrm{RMSE}}{\bar{x}}. \tag{3}$$

- The Pearson's correlation coefficient ($\rho$):

$$\rho = \frac{\mathrm{cov}(x, y)}{\sigma_x \cdot \sigma_y}. \tag{4}$$

**Table 1**
Correlation statistics for significant wave height and peak period between NC-GOW and buoy observations.

| | | | | $H_s$ (m) | | | | | $T_p$ (s) | | | | |
|---|---|---|---|---|---|---|---|---|---|---|---|---|---|
| Buoy name | Time span | Lon. | Lat. | $n$ | BIAS (m) | RMSE (m) | $\rho$ | SI | $n$ | BIAS (s) | RMSE (s) | $\rho$ | SI |
| BILBAO | 1990–08 | 356.95 | 44.00 | 49132 | 0.00 | 0.51 | 0.92 | 0.27 | 51517 | −0.72 | 2.13 | 0.79 | 0.22 |
| PENYAS | 1997–08 | 353.83 | 44.00 | 67365 | −0.24 | 0.66 | 0.85 | 0.34 | 68035 | −0.66 | 2.02 | 0.79 | 0.21 |
| ESTACA | 1996–08 | 352.38 | 44.06 | 62277 | 0.05 | 0.52 | 0.92 | 0.22 | 62471 | −0.69 | 2.13 | 0.78 | 0.22 |
| VILLANO | 1998–08 | 350.08 | 43.50 | 60848 | 0.03 | 0.55 | 0.91 | 0.23 | 60899 | −0.74 | 2.09 | 0.77 | 0.23 |
| SILLEIRO | 1998–08 | 350.61 | 42.13 | 39043 | 0.06 | 0.44 | 0.94 | 0.20 | 39184 | −0.74 | 1.92 | 0.78 | 0.20 |
| CADIZ | 1996–08 | 352.50 | 36.48 | 30755 | −0.08 | 0.60 | 0.71 | 0.49 | 35682 | −3.09 | 4.17 | 0.71 | 0.58 |
| CAR-41043 | 2007–08 | 294.99 | 20.99 | 14363 | 0.04 | 0.25 | 0.93 | 0.14 | 14363 | 0.33 | 1.43 | 0.79 | 0.16 |
| CAR-41040 | 2005–08 | 306.96 | 14.48 | 23060 | 0.07 | 0.26 | 0.90 | 0.13 | 23061 | 0.38 | 1.60 | 0.76 | 0.18 |
| CAR-41041 | 2005–08 | 313.99 | 14.36 | 28581 | 0.04 | 0.27 | 0.88 | 0.13 | 28581 | 0.30 | 1.75 | 0.78 | 0.20 |
| CH-32301 | 1984–86 | 254.80 | −9.90 | 3359 | 0.00 | 0.33 | 0.76 | 0.15 | 3359 | −0.98 | 3.46 | 0.71 | 0.29 |
| CH-32302 | 1986–95 | 274.90 | −18.00 | 68944 | 0.05 | 0.32 | 0.88 | 0.15 | 68939 | −0.20 | 3.07 | 0.71 | 0.24 |
| BER-46035 | 1985–07 | 182.42 | 57.05 | 158843 | −0.16 | 0.67 | 0.92 | 0.25 | 159523 | −0.37 | 2.73 | 0.67 | 0.30 |
| ALA-46003 | 1976–07 | 205.02 | 52.70 | 191687 | −0.15 | 0.66 | 0.92 | 0.22 | 185827 | −0.24 | 2.67 | 0.71 | 0.26 |
| ALA-46001 | 1972–07 | 211.83 | 56.30 | 234247 | 0.03 | 0.65 | 0.91 | 0.24 | 222623 | −0.50 | 3.20 | 0.65 | 0.32 |
| CAN-46004 | 1988–07 | 226.10 | 48.35 | 109988 | −0.22 | 0.77 | 0.89 | 0.27 | 109988 | −0.49 | 3.06 | 0.69 | 0.28 |
| NWUS-46005 | 1976–07 | 228.98 | 46.05 | 210187 | −0.19 | 0.59 | 0.93 | 0.21 | 201655 | −0.86 | 3.42 | 0.69 | 0.32 |
| NWUS-46006 | 1977–07 | 222.52 | 40.80 | 187124 | −0.14 | 0.57 | 0.94 | 0.20 | 179605 | −0.60 | 3.23 | 0.70 | 0.29 |
| HW-51001 | 1981–07 | 197.79 | 23.43 | 189167 | −0.02 | 0.40 | 0.91 | 0.17 | 189126 | −0.42 | 3.08 | 0.70 | 0.29 |
| HW-51002 | 1984–07 | 202.22 | 17.19 | 174107 | 0.07 | 0.43 | 0.84 | 0.18 | 174122 | −1.58 | 3.67 | 0.66 | 0.37 |
| HW-51003 | 1984–07 | 199.18 | 19.22 | 168201 | −0.01 | 0.37 | 0.87 | 0.17 | 168196 | −1.17 | 3.46 | 0.68 | 0.33 |
| HW-51004 | 1984–07 | 207.52 | 17.52 | 171378 | 0.02 | 0.38 | 0.85 | 0.16 | 171375 | −1.61 | 3.76 | 0.65 | 0.37 |

- where cov($x$,$y$) represents the covariance between the two variables and $\rho$ varies between −1 and 1.
- Sample distribution moments: means ($\bar{x}, \bar{y}$) and standard deviations ($\sigma_x$, $\sigma_y$).

These statistics are used to measure the quality of the results at the two validation stages:

1. Comparing numerical results (NC-GOW) with buoy data at a first stage.
2. Comparing calibrated numerical results (GOW) with buoy data and altimetry after the calibration process.

Due to the scattered distribution of buoy locations in the oceans, the only way to validate numerical results on a global scale is by comparing them with altimetry observations. To make meaningful comparisons, reanalysis data are interpolated to the instants and positions of the instrumental observations. For every node of the simulation grid, all altimetry observations within cells of the same dimension as the model resolution (1°×1.5°) are selected.

Fig. 2 shows scatter and quantile–quantile (25 equally distributed quantiles on a Gumbel scale) plots comparing buoy data and wave model results at different locations. In all cases, NC-GOW shows a good agreement. Note that in the case of the buoy CAR-41041, a tropical cyclone appears in the buoy record with a maximum significant wave height around 7 m, which is not appropriately reproduced by the wave model ($H_s$ around 2 m height). This is due to the poor resolution of the input wave fields. Note also that for high quantiles, wave heights appear to be under-estimated in some buoys while in others they are slightly over-estimated. This result supports the need of a correction, especially for the highest quantiles, which are the most relevant for engineering applications.

In Fig. 3, hindcast and instrumental $H_s$ time series of six different buoy locations, covering different years, are shown. For all cases, model data reproduces appropriately the magnitude and temporal evolution of the instrumental $H_s$ records. Note that the highest differences correspond to peak events, where some of them are accurately reproduced in magnitude while others are not. For instance, the peak events of NWUS-46006 buoy show little discrepancies during the first months of the year whereas differences up to 2 m occur for the last months of the year.

Fig. 4 shows the model performance on i) significant wave height ($H_s$), ii) peak period ($T_p$) and iii) mean wave direction ($\theta_m$) at Silleiro buoy station during year 2006. Note that besides $H_s$, both peak period and mean wave direction present very good agreement with respect to instrumental data. In general terms, we have found good agreement between model results and observations, and the higher discrepancies are associated with the highest wave events. This result is also observed, from a statistical point of view, in the quantile–quantile plots (see Fig. 2).

Table 1 provides for different buoy locations the following information: the name of the buoy, longitude and latitude, length of records ($n$), and several diagnostic statistics related to $H_s$ and $T_p$, respectively, comparing NC-GOW data versus buoy observations. From this validation the following remarks are pertinent:

1. The biases related to wave heights are relatively low. The highest absolute values correspond to negative biases, which means that the model overestimates wave heights on average.
2. The buoys located in areas with frequent storm (BER-46035, ALA-46003, NWUS-46006, CAN-46004 and NWUS-46005) tend to show a poorer performance in wave heights and are also associated with higher dispersion range (see scatter plots in Fig. 2).
3. The scatter indexes and correlation coefficients of $H_s$ are below 0.3 and above 0.85 respectively, which are appropriate diagnostic values for these kind of comparisons. Note that lower scatter indices and higher correlation coefficients correspond to higher reanalysis quality. Diagnostic statistics for CADIZ and CH-32301 (Chile) buoys are comparatively worse than for the rest of locations. The former is due to the coarse spatial grid resolution in semi-enclosed areas such as small gulfs and the latter may be due to the doubtful quality and short length (1984–1986) of the record.
4. Correlations related to the $T_p$ are lower than those associated with $H_s$. This result is consistent with results from other reanalyses existing in the literature.
5. The bias associated with $T_p$ is negative for all cases (overestimation of the model) except for the three buoys in the tropical Atlantic. This result is probably induced by (i) not enough swell dissipation in the model and (ii) the discrete interaction approximation (DIA) for non-linear wave interaction, which would also be consistent with the observed overestimate of the wave heights.

Caires et al., (2004) made a comparison of several global wind wave reanalysis, contrasting results during four different years (1978, 1988, 1994 and 1997) with several buoy records over the globe. Table 2 provides those results at the Peruvian coasts (buoy

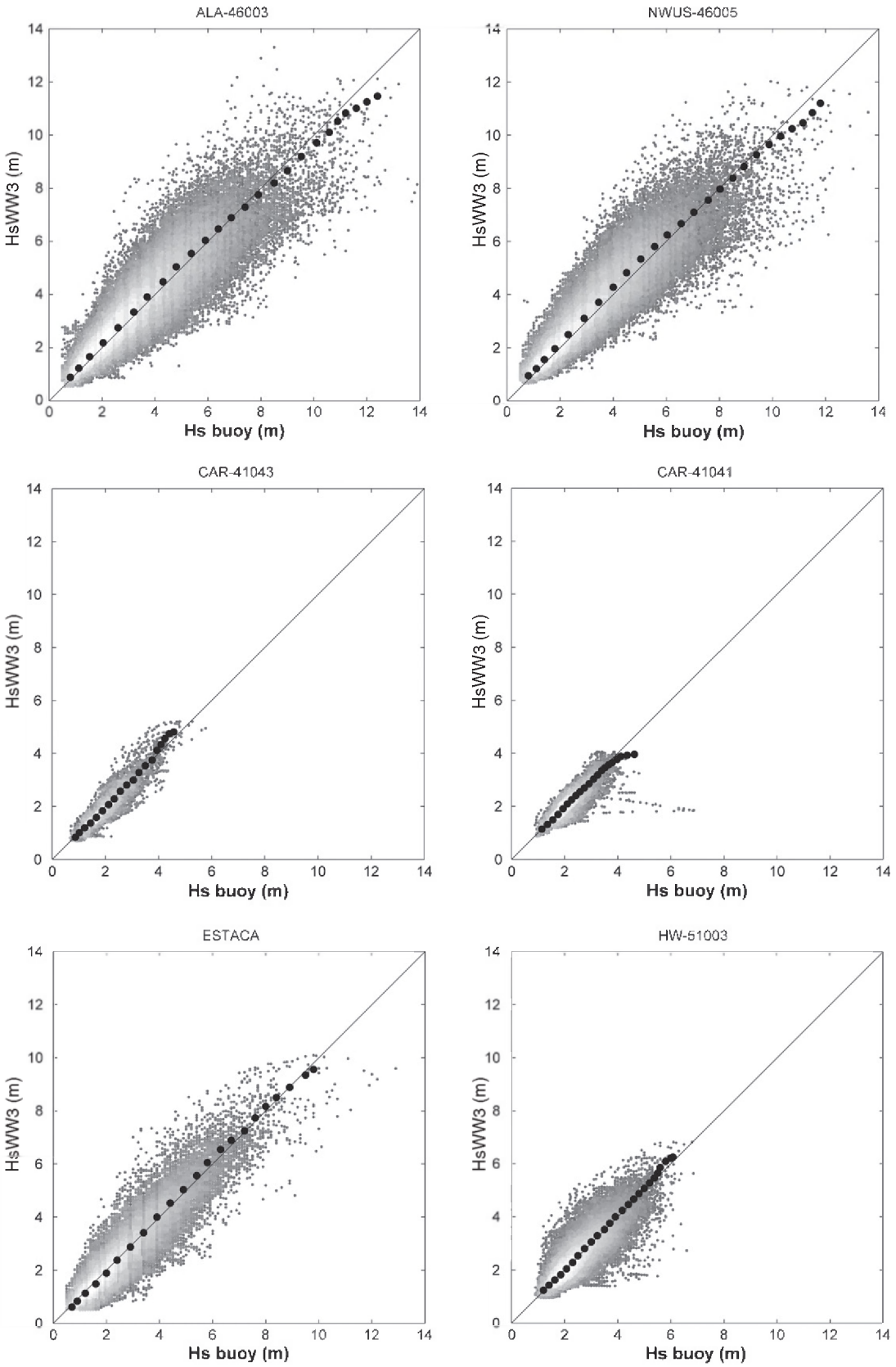


**Fig. 2.** Scatter and quantile–quantile plots of buoy measurements (horizontal axis) and wave model results (vertical axis). Large black dots represent the quantile values (plotted equally spaced in a Gumbel scale), small dots correspond to data pairs of significant wave heights (buoy versus model) and the color intensity represents the density of data. Data for each buoy correspond to the time span given in Table 1.

CH-32302), including also NC-GOW results for comparison purposes. Analogously, Tables 3 and 4 provide the same information as Table 2 but related to four islands in Hawaii (buoys HW-51001, HW-51002, HW-51003 and HW-51004) and three buoys close to the coast of Alaska (ALA-46001, ALA-46003 and CAN-46004), respectively. Note that their work did not include the comparison with more modern and better global reanalyses, like C-ERA-40 or ERA-Interim (Dee et al., 2011) datasets, this reason prevent us from making this comparison. It is important to note that expression (3) used for the Scatter Index in the present paper differs slightly from the one used in Caires et al., (2004):

$$SI_C = \frac{\sqrt{\frac{1}{n_d}\sum_{i=1}^{n_d}[(y_i-\bar{y})-(x_i-\bar{x})]^2}}{\bar{x}} = \frac{\sqrt{\frac{1}{n_d}\sum_{i=1}^{n_d}[(y_i-x_i)-\mathrm{BIAS}]^2}}{\bar{x}}, \quad (5)$$

however, they are equal ($SI_C = SI$) in case the BIAS is null. The comparison hereafter has been made with the $SI_C$ index.

In addition, there are some differences about how the data is pre-processed for comparison purposes. Caires et al., (2004) process the time series using the procedure described in Caires & Sterl, (2003), and compare reanalyses with a 6-h average from buoy observations. We compare 6 hour average data interpolated to the position and time (hourly) when the buoy records were registered, considering that the reanalysis winds are only available on a six hourly data. In this manner, the number of data (n) for comparison is of the same order than the reference. From results given in Tables 2, 3 and 4, the following observations are pertinent:

1. The mean values corresponding to ERA-40 and NC-GOW coincide for buoys on the Peruvian coast and Hawaii, and they are very close with respect to results in Alaska.
2. NC-GOW data preserves the quality of the correlation coefficients ($\rho$) and scatter indexes (SI).
3. NC-GOW gives lower BIAS results with respect to compared reanalyses for all locations.

Although results obtained from different reanalyses are not directly comparable due to pre-processing, our results are consistent with respect to analogous reanalyses and instrumental data, increasing the confidence on the NC-GOW performance. In addition, validation using buoy observations confirms the quality of the hindcast data related to: i) the time series evolution, and ii) the quantile statistical distribution.

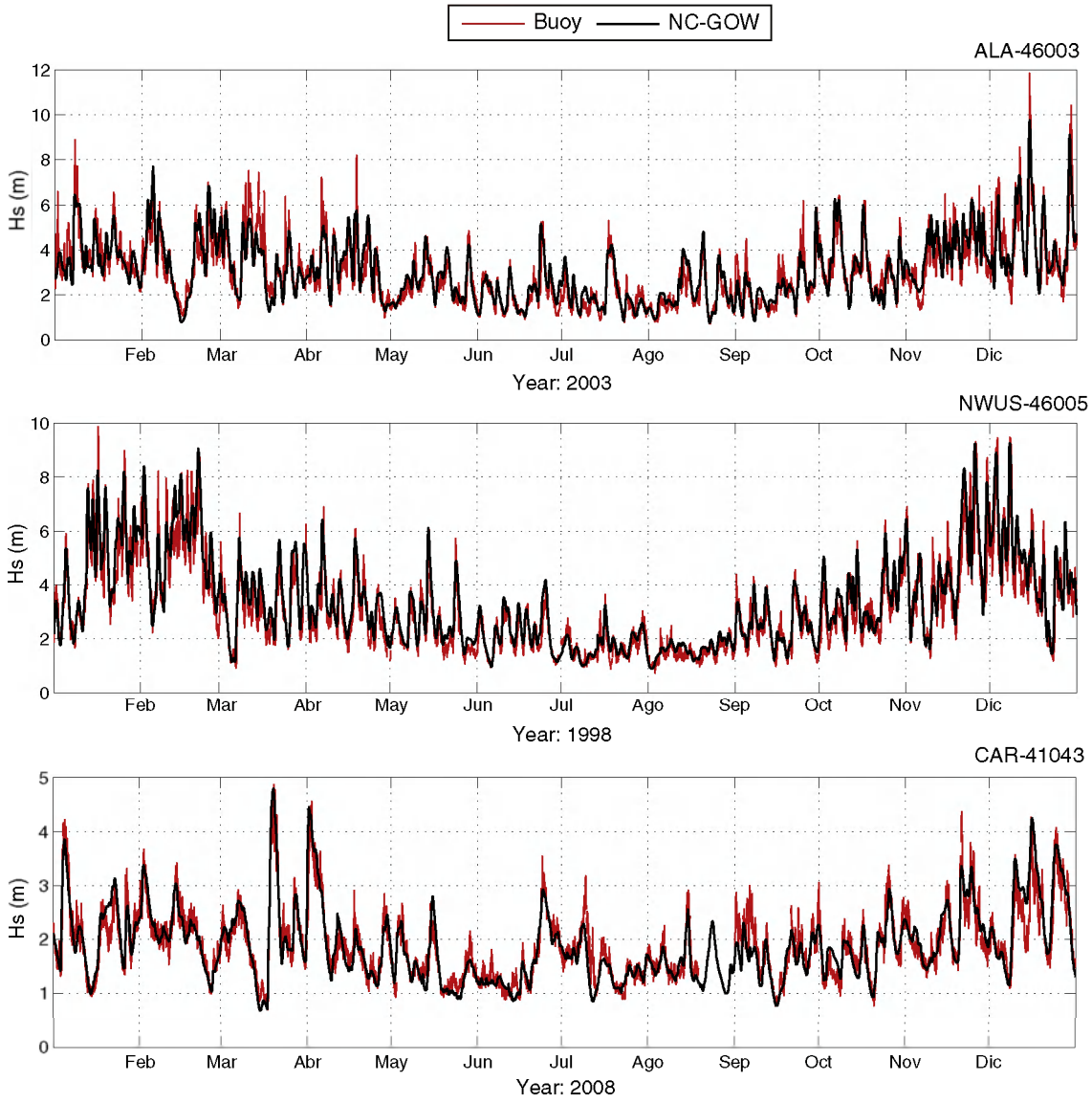


**Fig. 3.** Reanalysis (black) and instrumental (red) significant wave height ($H_s$) time series at several buoy locations. Data for each buoy correspond to the time span given in Table 1.

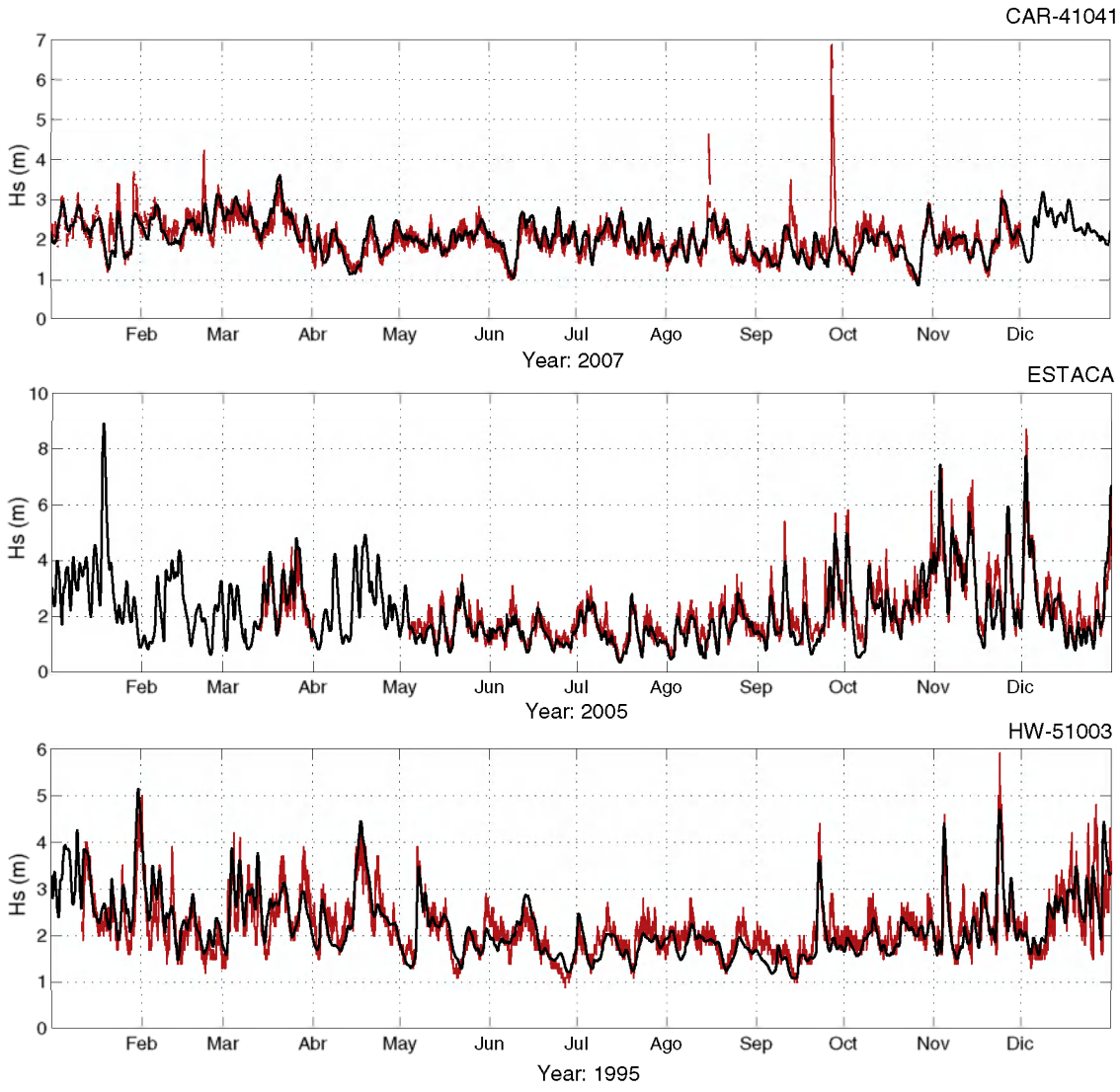


**Fig. 3** (*continued*).

Regarding the validation of NC-GOW on a global scale using altimetry data from 1992 up to 2008, Fig. 5 shows color plots of the mean and the 95th percentile $H_s$ for both altimetry and NC-GOW data. The storm tracks regions can be clearly identified, both in the Northern and Southern Hemisphere. Contour plots related to altimetry data present the same patterns as those associated with the NC-GOW data, which indicates that the model is properly describing the wave climate at a global scale. The larger differences are detected on those areas of higher significant wave heights, which are associated with high latitudes on both hemispheres.

Results indicate that Northern Hemisphere presents higher variability in wave climate conditions than the Southern Hemisphere. According to Izaguirre et al., (2011), by using satellite data, and Caires & Sterl, (2005a), by numerical modeling, the differences between average wave variations (variance) and extreme wave heights are larger in the Northern than in the Southern Hemisphere.

Visual inspection of Fig. 5 allows the identification of the same spatial patterns for both mean and 95th percentile values, which is a qualitative measure of the goodness of the dataset. In contrast, Fig. 6 shows the Pearson's correlation coefficient ($\rho$) for the hourly $H_s$ from 1992 to 2008. Note that diagnostic statistics are calculated removing outliers, i.e. data related to hurricanes and typhoons, using the method given in Mínguez et al., (2011b), which is briefly described in the next subsection. The higher and lower values for the correlation coefficient and scatter index, respectively, are obtained in areas of large mean significant wave heights (see Fig. 5). Comparatively worse correlation and scatter index results are obtained in tropical areas, big archipelagos and semi-enclosed basins. The same conclusion is reached if different statistics, such as RMSE and Bias, are used instead (not shown due to space limitations). The discrepancies between numerical and altimetry data sets, especially in those areas where reanalysis is more limited due to the temporal and spatial resolution, justify the application of additional corrections to embed instrumental information.

### 2.5. Wave field corrections procedures

Validation results given previously show the good performance of the wave reanalysis with respect to: i) analogous reanalysis existing in the literature, and ii) instrumental data (buoys and altimetry). These characteristics make this reanalysis a useful design tool for offshore and coastal structures, since it offers long continuous time series and good spatial coverage for the statistical characterization of wave climate with respect to other sources of information. However, several authors (see Caires & Sterl, (2005b), Cavaleri & Sclavo, (2006), Mínguez et al., (2011a) or Mínguez et al., (2011b)) point out that

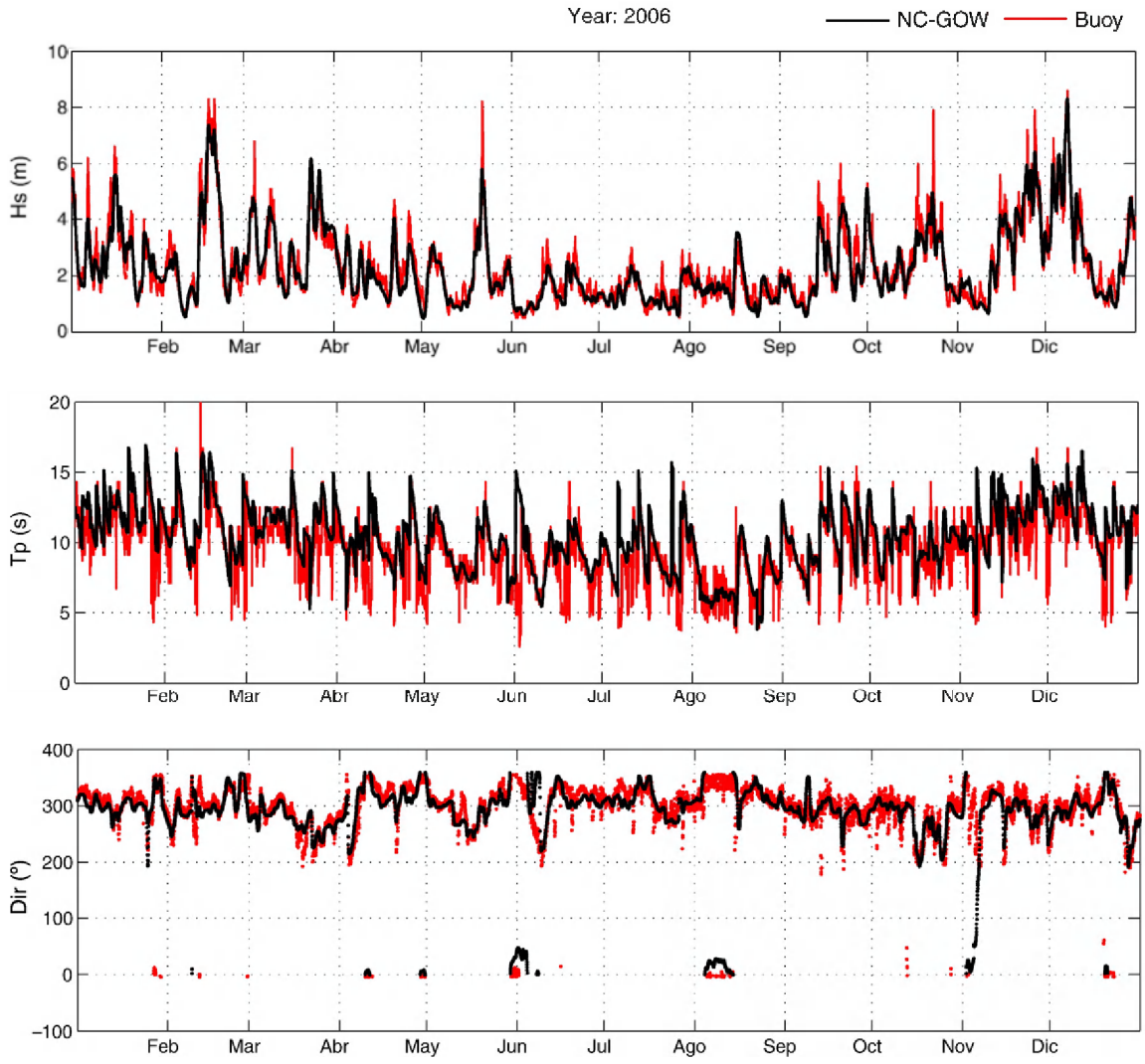


**Fig. 4.** Time series of significant wave height ($H_s$), peak period ($T_p$) and mean wave direction ($\theta_m$) at SILLEIRO buoy. Red: buoy measurement, Black: wave model.

there are still discrepancies when comparing WRD with instrumental data. These differences are mainly provoked by insufficient forcing resolution, and it becomes more evident in the presence of hurricanes and typhoons, which make instrumental data to appear as outliers.

In order to improve robustness of the reanalysis and configure the GOW database, a calibration procedure based on Mínguez et al., (2011a) is performed using altimetry instrumental data. Previous to calibration, an outlier filter (see Mínguez et al., (2011b)) is applied to remove instrumental data related to hurricanes and typhoons. These two procedures are briefly described in the following sections.

**Table 2**
Comparison in Peruvian coast for several wave reanalysis (modified from Caires et al., (2004)).

| Year | REAN | $n$ | Mean (m) | BIAS (m) | RMSE (m) | $\rho$ | $SI_C$ |
|---|---|---|---|---|---|---|---|
| 1988 | ERA-40 | 1461 | 2.21 | −0.03 | 0.33 | 0.84 | 0.15 |
| | ERA-40/ODGP2 | | | −0.30 | 0.41 | 0.87 | 0.13 |
| | CS01 | | | −0.24 | 0.40 | 0.83 | 0.15 |
| | PWA-R | | | −0.14 | 0.38 | 0.84 | 0.16 |
| | NC-GOW | 1410 | 2.22 | −0.03 | 0.28 | 0.90 | 0.12 |
| 1994 | ERA-40 | 1457 | 2.18 | −0.14 | 0.30 | 0.92 | 0.12 |
| | CS01 | | | −0.43 | 0.56 | 0.82 | 0.17 |
| | PWA-R | | | −0.33 | 0.48 | 0.83 | 0.16 |
| | NC-GOW | 1412 | 2.18 | 0.13 | 0.32 | 0.89 | 0.14 |

### 2.6. Identification and removal of outliers

The bad performance during hurricanes and typhoons, which can be observed in the scatter plot of CAR-41041 in Fig. 2 and in the corresponding time series in Fig. 3, is produced because the tropical cyclones are not appropriately resolved using WW3, due to the resolution of the input wind fields. Note that failing to exclude those outlier observations may provoke the distortion of any

**Table 3**
Comparison in Hawaii for several wave reanalysis (modified from Caires et al., (2004)).

| Year | REAN | $n$ | Mean (m) | BIAS (m) | RMSE (m) | $\rho$ | $SI_C$ |
|---|---|---|---|---|---|---|---|
| 1988 | ERA-40 | 3399 | 2.20 | −0.23 | 0.42 | 0.87 | 0.16 |
| | ERA-40/ODGP2 | | | −0.31 | 0.45 | 0.87 | 0.15 |
| | CS01 | | | −0.16 | 0.40 | 0.83 | 0.17 |
| | PWA-R | | | −0.45 | 0.62 | 0.81 | 0.19 |
| | NC-GOW | 4013 | 2.20 | 0.04 | 0.37 | 0.86 | 0.17 |
| 1994 | ERA-40 | 4570 | 2.55 | −0.38 | 0.51 | 0.90 | 0.13 |
| | CS01 | | | −0.46 | 0.62 | 0.81 | 0.17 |
| | PWA-R | | | −0.59 | 0.73 | 0.83 | 0.17 |
| | NC-GOW | 4342 | 2.55 | 0.18 | 0.46 | 0.85 | 0.17 |
| 1997 | ERA-40 | 5569 | 2.37 | −0.16 | 0.35 | 0.90 | 0.13 |
| | CS01 | | | −0.31 | 2.48 | 0.85 | 0.15 |
| | PWA-R | | | −0.37 | 0.58 | 0.84 | 0.19 |
| | NC-GOW | 6820 | 2.34 | −0.03 | 0.39 | 0.86 | 0.17 |

**Table 4**
Comparison in Alaska buoys for several wave reanalysis (modified from Caires et al., (2004)).

| Year | REAN | $n$ | Mean (m) | BIAS (m) | RMSE (m) | $\rho$ | SI$_C$ |
|---|---|---|---|---|---|---|---|
| 1978 | ERA-40 | 3313 | 2.54 | −0.24 | 0.38 | 0.90 | 0.29 |
| | CS01 | | | 0.35 | 0.48 | 0.86 | 0.31 |
| | NC-GOW | 1134 | 2.49 | −0.45 | 0.70 | 0.88 | 0.22 |
| 1988 | ERA-40 | 4054 | 3.18 | −0.35 | 0.68 | 0.94 | 0.18 |
| | ERA-40/ODGP2 | | | −0.14 | 0.57 | 0.93 | 0.18 |
| | CS01 | | | 0.29 | 0.71 | 0.92 | 0.20 |
| | PWA-R | | | −0.14 | 0.80 | 0.91 | 0.25 |
| | NC-GOW | 3139 | 3.07 | −0.03 | 0.60 | 0.93 | 0.20 |
| 1994 | ERA-40 | 3793 | 2.91 | −0.37 | 0.60 | 0.97 | 0.16 |
| | CS01 | | | 0.20 | 0.59 | 0.94 | 0.19 |
| | PWA-R | | | −0.17 | 0.70 | 0.93 | 0.24 |
| | NC-GOW | 2700 | 2.98 | −0.07 | 0.60 | 0.94 | 0.20 |
| 1997 | ERA-40 | 3788 | 2.87 | −0.21 | 0.50 | 0.96 | 0.16 |
| | CS01 | | | 0.20 | 0.65 | 0.92 | 0.22 |
| | PWA-R | | | −0.22 | 0.75 | 0.91 | 0.26 |
| | NC-GOW | 3684 | 2.81 | −0.08 | 0.61 | 0.92 | 0.21 |

corrective action. Besides, these data should be treated and analyzed separately for the results of the correction to be fully reliable. For this reason we apply an outlier filter to eliminate these unresolved processes.

Mínguez et al., (2011b) present different outlier detection regression techniques applied to WRD. The methods are intended for an automatic hurricane and typhoon identification. The advantage of using any of these techniques are: i) it allows the identification and removal of $H_s$ related to tropical storms, inappropriately reproduced by the reanalysis, ii) it does not require the availability of a tropical storm database, and iii) it allows the identification of areas where the influence of tropical storms are relevant, which should be further studied using appropriate models, higher temporal and spatial resolution, etc.

For this particular case, we have selected the method based on a nonlinear heteroscedastic regression model because it is robust and the parameterization is flexible to be applied on different wave climates, which is particularly important as the filtering is applied all over the grid. The model can be expressed in the form:

$$y_i = f_\mu(x_i;\beta) + \varepsilon_i, \quad i = 1,2,\ldots,n, \tag{6}$$

where $x_i$ corresponds to the $i$th predictor variable (interpolated hindcast data), and $y_i$ is the $i$th value of the response variable (instrumental data). The model mean and standard deviation are parametrized as follows:

$$f_\mu(x_i,\beta) = \beta_0 x_i^{\beta_1} \tag{7}$$

$$\sigma(x_i,\gamma) = \gamma_0 x_i^{\gamma_1}, \tag{8}$$

where $\beta$ and $\gamma$ are parameter vectors related to the model mean (7) and standard deviation (8), respectively. Note that the standard deviation heteroscedasticity is modeled through the nonlinear function (8), and $\varepsilon_i; i=1, \ldots, n$ are jointly normally distributed $\varepsilon \sim N(0, \sigma_i)$ errors.

Once data pairs (instrumental versus reanalysis) are selected, the outlier identification technique encompasses the following steps:

1. Estimate the parameters $\beta_0$, $\beta_1$, $\gamma_0$ and $\gamma_1$ using the method of maximum likelihood.
2. Calculate the residual vector:

$$\hat{\varepsilon} = y - f_\mu\left(x;\ \hat{\beta}\right), \tag{9}$$

where the tilde " ^ " refers to estimated values.

1. Obtain the residual variance-covariance matrix $\Omega$ using a first-order Taylor series expansion of the regression model at the optimum.
2. Compute the studentized residuals as follows

$$z_i = \frac{\hat{\varepsilon}_i}{\sqrt{\Omega_{i,i}}} = \frac{y_i - f_\mu\left(x_i;\ \hat{\beta}\right)}{\sqrt{\Omega_{i,i}}} \quad i = 1,\ldots,n, \tag{10}$$

where $\Omega_{i,i}$ is the $i$th diagonal element of $\Omega$.

1. Outlier identification: For a given confidence level, i.e. $\alpha = 0.0001$, any case is identified as an outlier if $|z_i| > \Phi^{-1}(1-\alpha/2)$.

For the purpose of this study, simulation and sensitivity tests performed in (Mínguez et al., 2011b), allow us to set the significance level to $\alpha = 0.0001$, for an appropriate removal of data associated with hurricanes and typhoons.

Fig. 7 presents an example of filtering for a particular location close to the Caribbean sea, which is an area where the presence of hurricanes and tropical storms is highly frequent. The figure shows the scatter plot, empirical and fitted regression model, and information the data removed for different confidence levels. Black dots in the scatter plot indicate those points detected as outliers using a significance level of $\alpha = 0.0001$. Note that there are instrumental significant wave heights above 7 m which do not exceed 3 m within the hindcast. Those points are related to high values of standardized residuals and are removed for calibration purposes. Alternation in colors indicate data located between different significance levels.

### 2.7. Wave height calibration

Even though there has been an important improvement in numerical wave generation models, validation of results still present discrepancies with respect to instrumental data. There are several reasons, such as a bad descriptions of wind fields and insufficient forcing and model resolution (Feng et al., 2006). Additional factors also contribute to poor model performance on shallow waters, such as, inappropriate shallow water physics in wave models, unresolved island blocking, imperfect bathymetry, etc. (see Cavaleri et al., (2007) for a summary). For this reason, several attempts to correct wave heights with instrumental data has been presented in the literature.

Caires & Sterl, (2005a) propose a relation between buoy and ERA-40 wave data for the 100-year return values, based on a nonparametric method with "analogs" from a learning dataset. Tomás et al., (2008) present a spatial calibration method based on empirical orthogonal functions. More recently, Mínguez et al., (2011a) presents a calibration procedure which depends on mean directions. Once the outliers have been identified and removed, we use the method proposed by Mínguez et al., (2011a) to embed satellite information in the GOW database. The calibration procedure is based on measurements during satellite age and the correction is applied for the full period of wave hindcast. This assumption can be considered suitable for engineering applications since statistics are corrected. Spatial caution must be taken for climate variability analysis however.

The model can be mathematically expressed as:

$$H_s^C = a^R(\theta)\left[H_s^R\right]^{b^R(\theta)} \tag{11}$$

where $H_s^R$ is the reanalysis significant wave height, $H_s^C$ is the calibrated or corrected significant wave height, and $a^R(\theta)$ and $b^R(\theta)$ are the parameters dependent on the mean wave direction $\theta$ from reanalysis. Note that for sea states with multiple components this correction does not consider the different directions of each component and its effect should be further explored depending on the relative

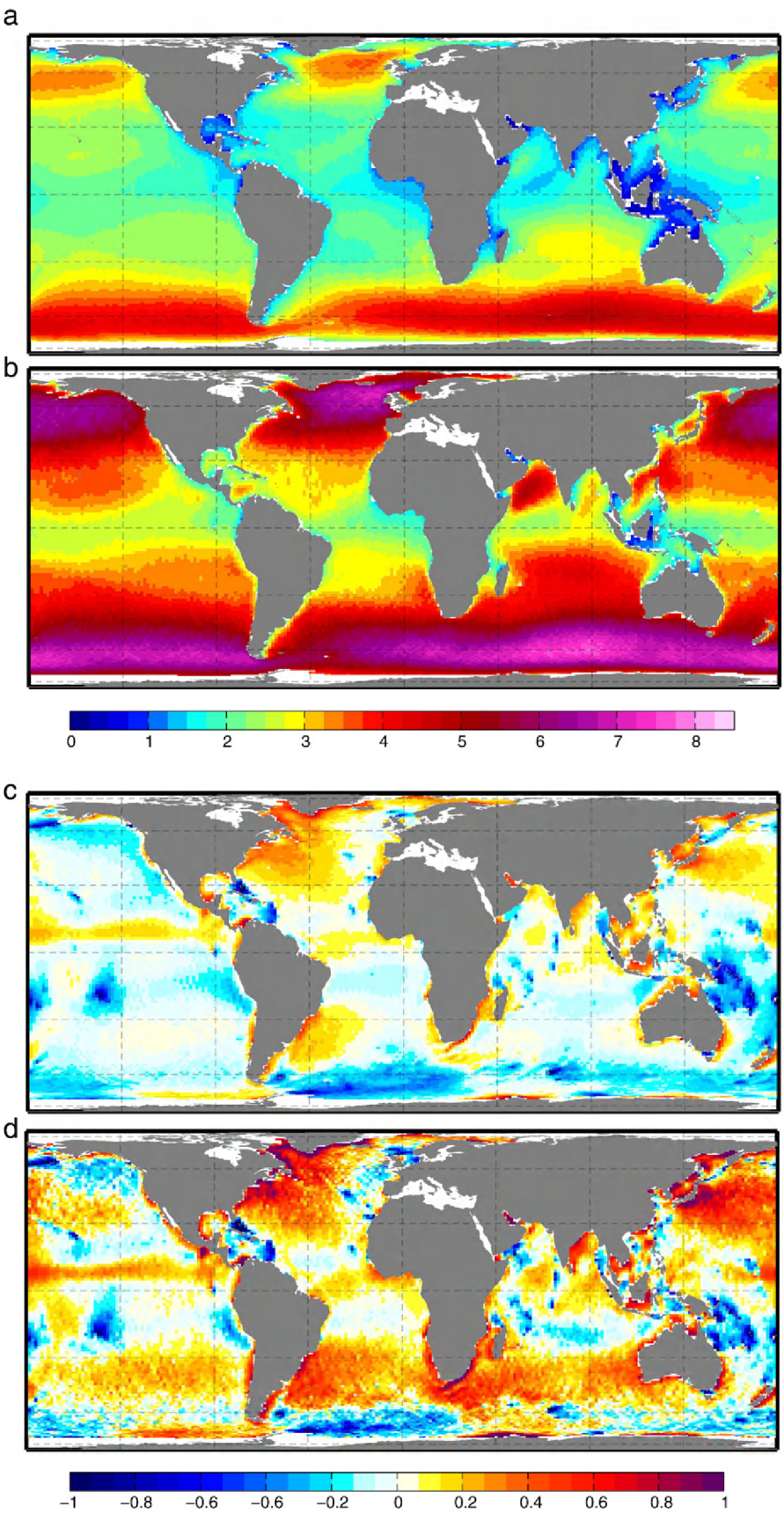


**Fig. 5.** Mean and 95th percentile of significant wave height from NC-GOW hindcast data (panels a and b respectively) and differences with altimeter satellite data ([SAT] − [NC-GOW]) for both statistics from 1992 to 2008 (panels c and d, respectively).

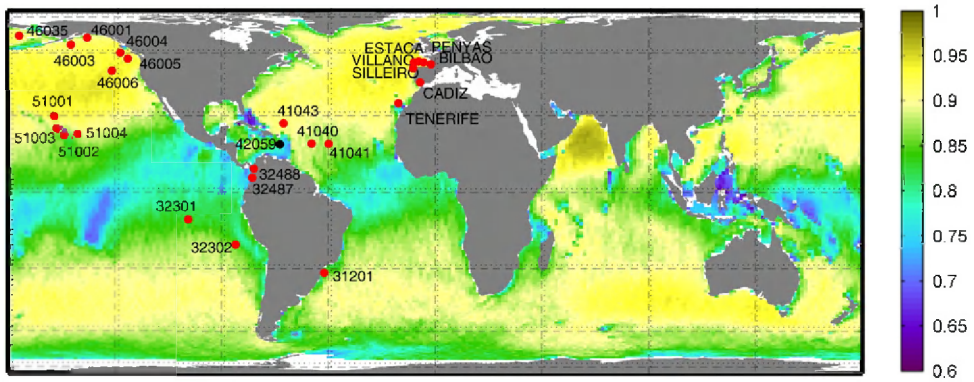


**Fig. 6.** Global map of Pearson correlation coefficient between satellite observations and hindcast results (NC-GOW) for the full period of available altimetry observations (1992–2008). Red dots represent buoy locations.

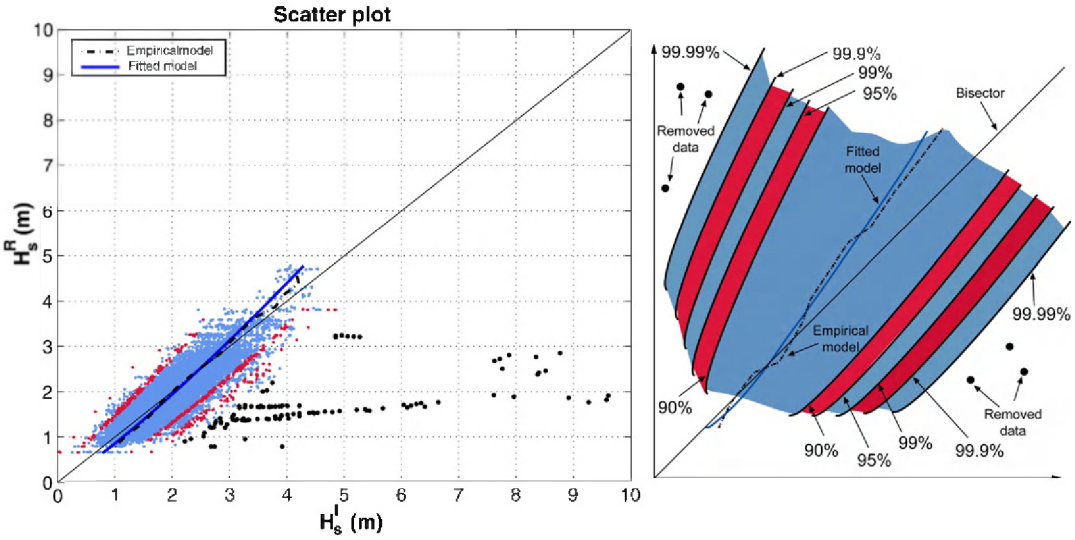


**Fig. 7.** Significant wave height outlier identification scatter plot (buoy versus model) in one location near the Caribbean affected by hurricanes. Black dots represent the identified outliers and blue and red dots correspond to data at different confidence levels (see legend in the right panel). The black discontinuous line depicts the empirical quantile distribution and the blue solid line the quantiles for the fitted model.

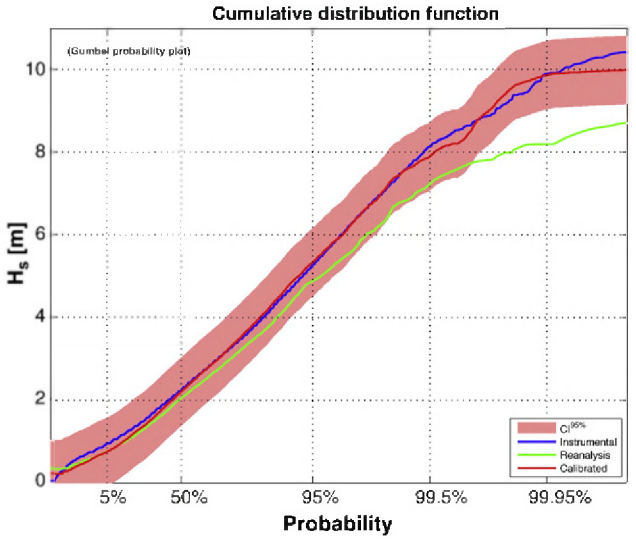


**Fig. 8.** Diagnostic plot for the calibration process for one particular location. Blue, green and red lines represent, respectively, the cumulative distribution function of instrumental, model and calibrated significant wave heights. Red shadowing correspond to the 95% confidence calibrated confidence bounds.

importance of each energetic component. This deficiency on the calibration process is also acknowledged in Mínguez et al., (2011a).

The parameter values for all possible directions are obtained by interpolation using smoothing cubic spline functions:

$$a_i^R(\theta_i) = a_j + x_j^a\left(\theta_i - \theta_j\right) + y_j^a\left(\theta_i - \theta_j\right)^2 + z_j^a\left(\theta_i - \theta_j\right)^3, \tag{12}$$

$$b_i^R(\theta_i) = b_j + x_j^b\left(\theta_i - \theta_j\right) + y_j^b\left(\theta_i - \theta_j\right)^2 + z_j^b\left(\theta_i - \theta_j\right)^3, \tag{13}$$

where $a_i^R$ and $b_i^R$ are the interpolated model correction parameters for a given direction $\theta_i$, $a_j$, $b_j$; $j = 1, \ldots, n_p$ are the parameters to be estimated, i.e. the parameter values associated with directions $\theta_j$; $j = 1, \ldots, n_d$, and $x_j^a$, $y_j^a$, $z_j^a$, $x_j^b$, $y_j^b$, $z_j^b$; $j = 1, \ldots, n_d$ are the corresponding cubic spline parameters, which are obtained using zero, first and second order continuity conditions along the circumference ($0 \le \theta \le 2\pi$).

Model parameters $a_j$, $b_j$; $j = 1, \ldots, n_p$ are estimated using the least squares method. Once these parameters are obtained it is possible to correct the complete reanalysis time series using mean wave direction records and expression (11). The calibration method makes the directional correction based on quantiles on a Gumbel scale, which gives more importance to the upper tail of the wave heights distribution. Note that for this reason the outlier removal is necessary, because if there exists data related to hurricanes or typhoons they will

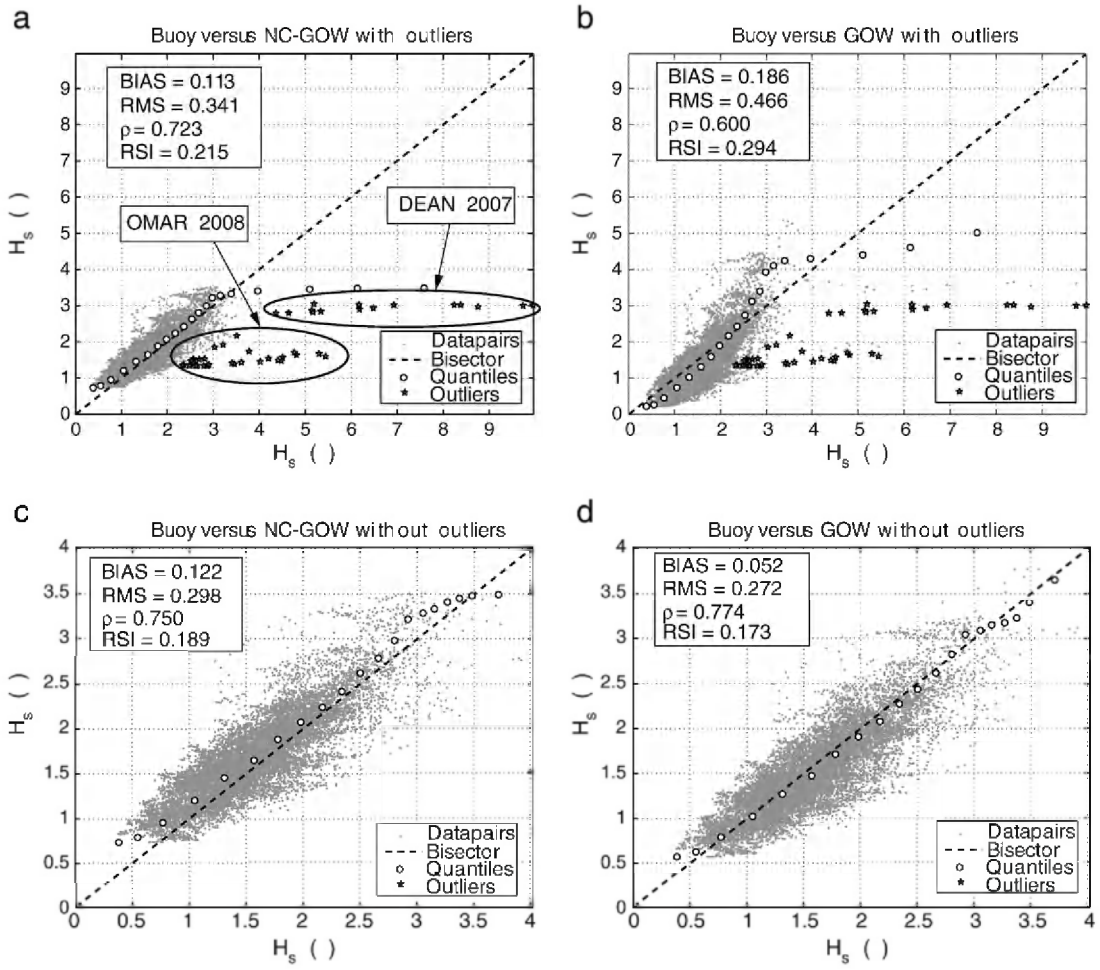


**Fig. 9.** Scatter and quantile–quantile plots before (a, c) and after (b, d) the calibration process, without the outlier identification (a, b) and after the removal of the outliers (c, d). Outliers due to Dean and Omar hurricanes are outlined in panel a.

present discrepancies with instrumental data and the calibration may distort model data misguidedly all over the quantile range in the attempt to correct the discrepancies, as seen in Fig. 8. For more details about the methodology and its hypothesis see Mínguez et al., (2011a).

Fig. 8 presents the calibration results for the same example used in Fig. 7 after outlier removal. The figure shows the cumulative distribution functions of instrumental, NC-GOW and GOW data including 95% confidence bands on a Gumbel probability plot. Although the performance for buoy data previously shown did not improve significantly, the empirical cumulative distribution function (ecdf) related to calibrated data is closer to the instrumental ecdf, especially in the upper tail of the distribution. Calibrated results always present better agreement from a statistical viewpoint.

Fig. 9 shows the relevance of outliers filter in the calibration procedure for a buoy (NOAA, 42059: 15.054° N, 67.47° W) located in the Caribbean sea. The $H_s$ scatter and quantile–quantile plots of instrumental versus calibrated reanalysis, after (right panels: b, d) and before (left panels: a, c) calibration, are shown without no removal of outliers (upper panels: a, b) and after applying the outlier filter (lower panels: c, d). Hurricanes Dean (year 2007) and Omar (year 2008) have been remarked in the upper-left panel (a). Note

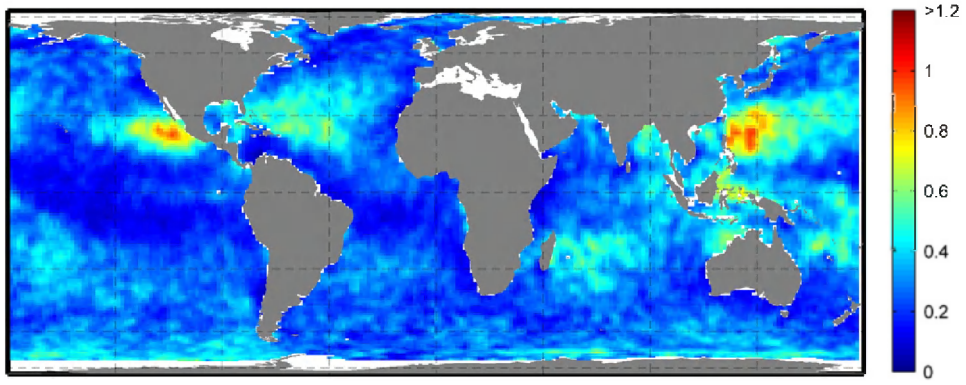


**Fig. 10.** Spatial distribution of the percentage of outliers removed at each location within GOW domain, for a given confidence level $\alpha = 0.0001$.

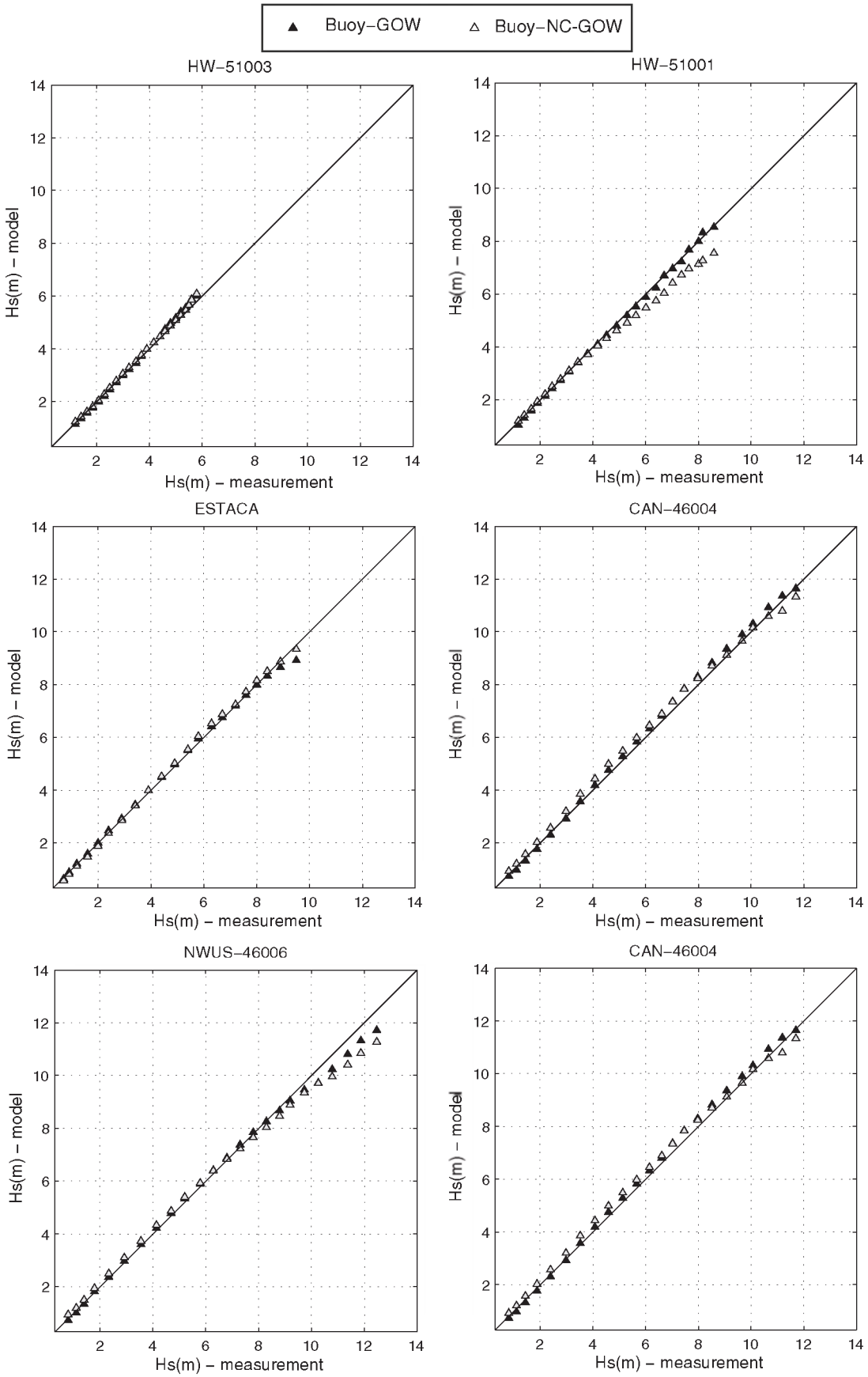


**Fig. 11.** Quantile distributions before and after the calibration process at several buoys (plotted equally spaced in a Gumbel scale).

that for Omar hurricane, instrumental wave heights between 3 and 5 m correspond to model wave heights between 1.2 and 2.5 m, and also instrumental wave heights above 7 m for Dean do not exceed 3 m in the model. These circumstances provoke the highest four quantiles to move away from the bisector. If the calibration procedure is applied without removing those observations which are not properly resolved in the model, results given in the upper-right panel rred(b) are obtained. Note that the calibration process deteriorates results, obtaining worse diagnostic statistics with respect to reanalysis data, i.e. higher bias, root mean square error and scatter index, and lower correlation coefficient. However, if the outlier filter is applied previously to make the calibration, the scatter and quantile–quantile plots, shown in the lower-left panel (c) of Fig. 9, are obtained, which after the calibration process transforms into results shown in the lower-right panel (d) of Fig. 9. Diagnostic statistics after the calibration process improve, i.e. lower bias, root mean square error and scatter index, and higher correlation coefficient.

Fig. 10 shows the number of data suspicious to be outliers for a significance level $\alpha = 0.0001$ all over the GOW grid domain. Note that the larger values are located in areas where the occurrence of hurricanes, typhoons and tropical cyclones is frequent. Reanalysis data over those locations should be used with care if high values of significant wave heights are analyzed.

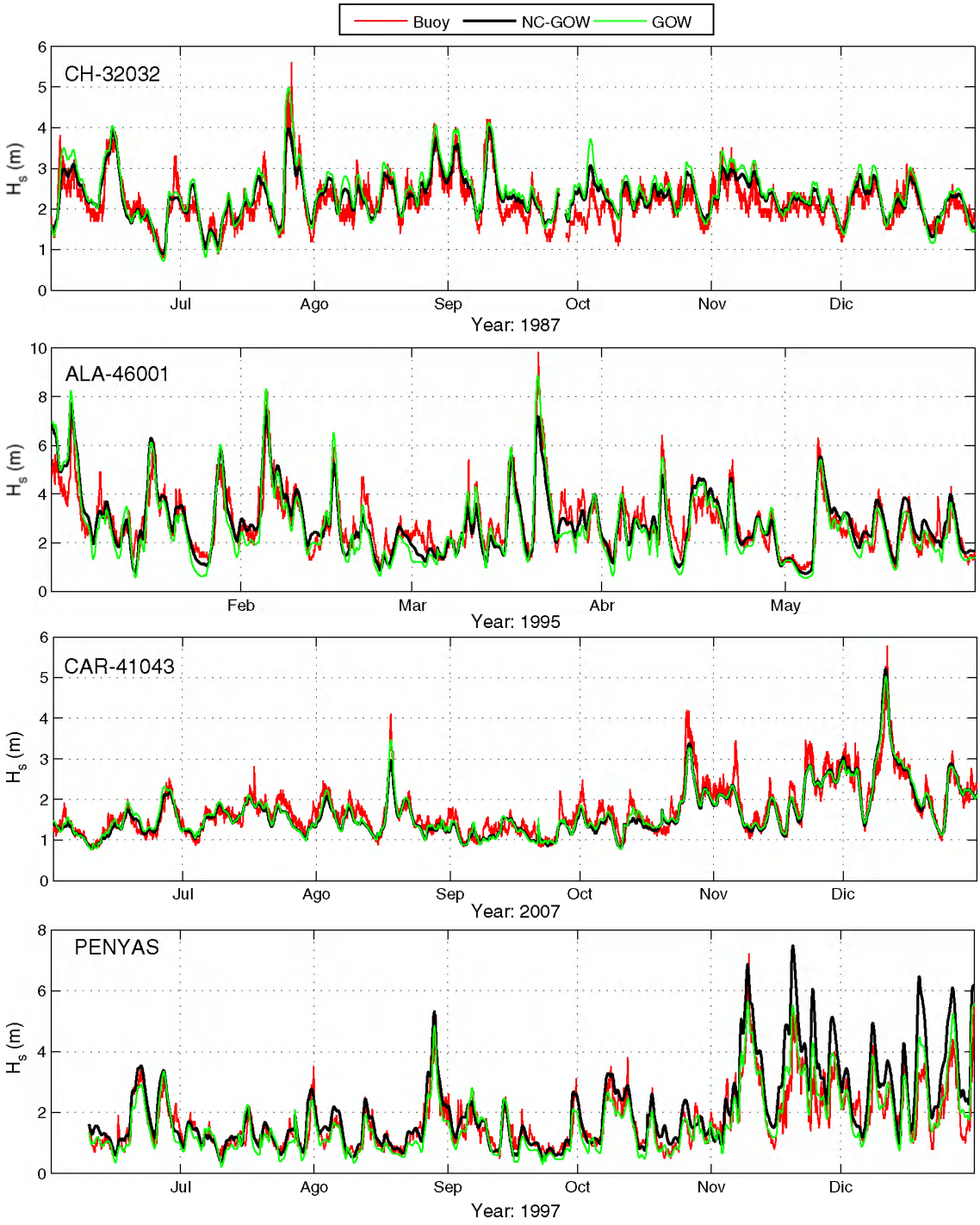


**Fig. 12.** Buoy (red), NC-GOW (black) and GOW (green) significant wave height ($H_s$) time series at several locations.

## 3. The GOW wave reanalysis

As mentioned in the previous section, the calibration is applied to each node of the simulation grid using the satellite data cells. In order to further compare the effect of the calibration process, we have applied the calibration method using several buoy time series records, as shown in Fig. 11, where different quantiles before and after the calibration process are provided. Note that although reanalysis quantiles present good agreement with respect to buoy time series quantiles, the calibration process improves results, especially in the upper part of the distribution, with the exception of the extreme tail at ESTACA buoy. The calibration is applied using the estimated parameters of calibration of the closest reanalysis grid node, and using instrumental data. This result reinforces the consistency of the calibration method.

Fig. 12 shows $H_s$ time series related to i) buoy (red line), ii) NC-GOW hindcast (black line), and iii) GOW (green line), for different buoys over different years (1987, 1995, 1997, and 2007). The corrected record maintains the concordance in the temporal fluctuations and do not imply significant changes in magnitude for the CH-32302 buoy. For the ALA-46001 station, the calibration process improves the storm peak value occurred in March 1995. It is worth noting the higher variability observed in the buoy CAR-41043 record. This effect is probably produced by the variability of winds below the 6 hour temporal resolution of the wind database. Note that despite the correction, the time series differences during October remain unsolved. Related to PENYAS time series record, the improvement of the calibration process implies a decrease of storm peaks.

The influence of the calibrated procedure for the annual mean and the 95th percentile of $H_s$ is shown in Fig. 13. As can be seen, the GOW wave reanalysis is able to model adequately those parameters that is also presented.

Comparison with buoy records does not provide the spatial verification of how the correction performs. For this reason, next section presents the verification of the calibration process, analyzing the spatial distribution of: i) correlation statistics and ii) wave parameters.

The verification of the calibration method is presented based on an analysis of the performance by using altimetry data available from 1992 to 2005 (training set) for calibration parameter estimation purposes. These estimated parameters allow comparison of calibrated times series from 2006 to 2008 with respect to altimetry observations during the same period (verification set). This verification is needed

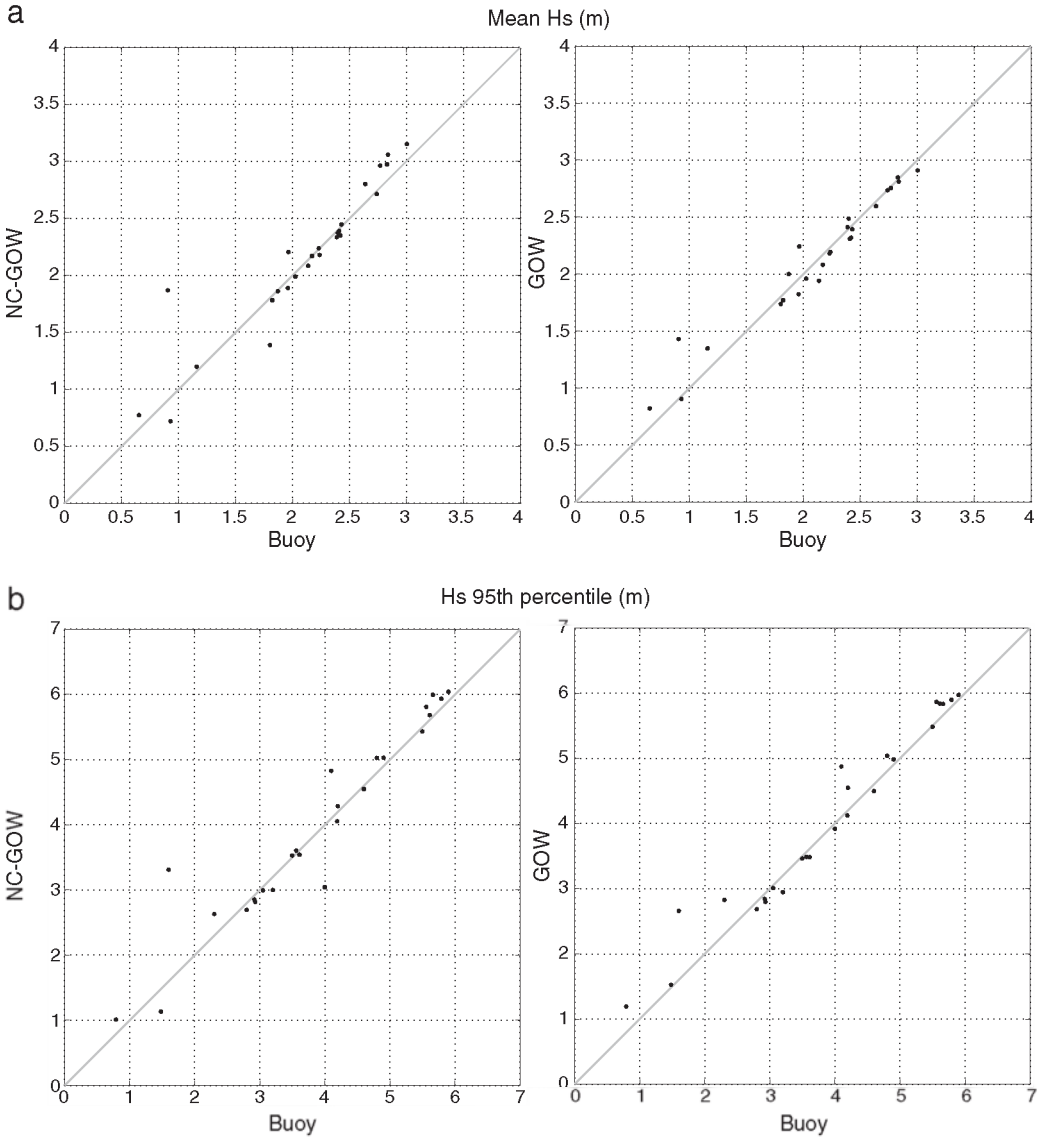


**Fig. 13.** Comparison of (a) annual mean significant wave height and (b) 95th percentile, between buoy data from Table 1 with respect to NC-GOW (left panels) and GOW (right panels) data, respectively.

in order to compare the corrected wave heights in a global domain and not only in scattered locations.

Fig. 14 represents the difference in the 95th percentile of $H_s$ between altimetry versus NC-GOW hindcast and altimetry versus GOW for the verification set of data. The areas where the differences are higher previous to calibration correspond to high latitudes, and coastal and island areas. Over these areas, where there are differences up to 1.5 m height, the calibration process reduces this difference to less than 0.5 m height. The higher differences after corrections are found in the Southern Hemisphere, which on average presents lower discrepancies previous to calibration with respect to altimetry data. The mean difference in the Northern Hemisphere is about −0.174 m for the 95th percentile (model underestimation), which is reduced to 0.017 m after the calibration process. In the Southern Hemisphere, the difference decreases from −0.064 to 0.020 m. Considering data on a global scale, mean differences change from −0.106 before calibration to 0.019 m afterwards. The mean significant wave height differences are lower than those obtained for the 95th percentile which decrease from 0.026 to −0.008 m after calibration.

The absolute change in $H_s$ although important may not be completely representative of the effect of the calibration because the wave conditions vary considerably in latitude (see Fig. 5) and in areas with higher waves the differences are expected to be greater, while in relative terms the effect can be not so noticeable. For this reason, Fig. 15 focuses only on the transformation of the simulated results, before and after the calibration, in terms of difference and relative change. The critical zones, where the effect of the correction is more important, can be clearly identified: high latitudes in the Atlantic and Pacific Oceans and coastal and island influenced areas. Note that it is in these coastal and island areas where the correlation statistics presented the worst agreement with respect to instrumental data, and for this reason, the percentage of change is higher.

In terms of correlation statistics, Fig. 16 shows the global maps of the RMSE of $H_s$ (m) before and after the calibration for the verification period. Again, the areas with higher discrepancies with respect to altimetry observations can be clearly identified, as previously remarked in Fig. 6 for the full period of the altimetry data. After the calibration, the results improve considerably in the areas that were incorrect and remains the same in most of the domain where the reanalysis data was satisfactory. In global average values, RMSE decreases from 0.554 to 0.529, SI from 0.219 to 0.206, the BIAS from −0.026 to 0.008 m and the correlation coefficient increases from 0.869 to 0.873. In global terms this change is not very significant, but the improvement in coastal regions is remarkable.

From the verification analysis, we can conclude that: (1) after the calibration, the differences with altimetry observations are reduced, (2) larger wave heights are more affected by the correction; (3) critical areas that showed the worst agreement with observations are corrected with the calibration method, (4) coastal regions are considerably improved; and (5) the correction performance is supported by the improvement achieved when comparing with respect to altimetry and buoy data.

## 4. Conclusions

We have presented a global wave dataset simulated with the model WaveWatchIII and driven by the NCEP/NCAR reanalysis winds and ice fields, covering the period from 1948 to 2008, which may be periodically updated.

Based on the application of a calibration method the dataset has been corrected using altimetry data from the period from 1992 to 2008. The outliers due to tropical cyclones are not appropriately reproduced in the simulation process, due to lack of resolution in the wind

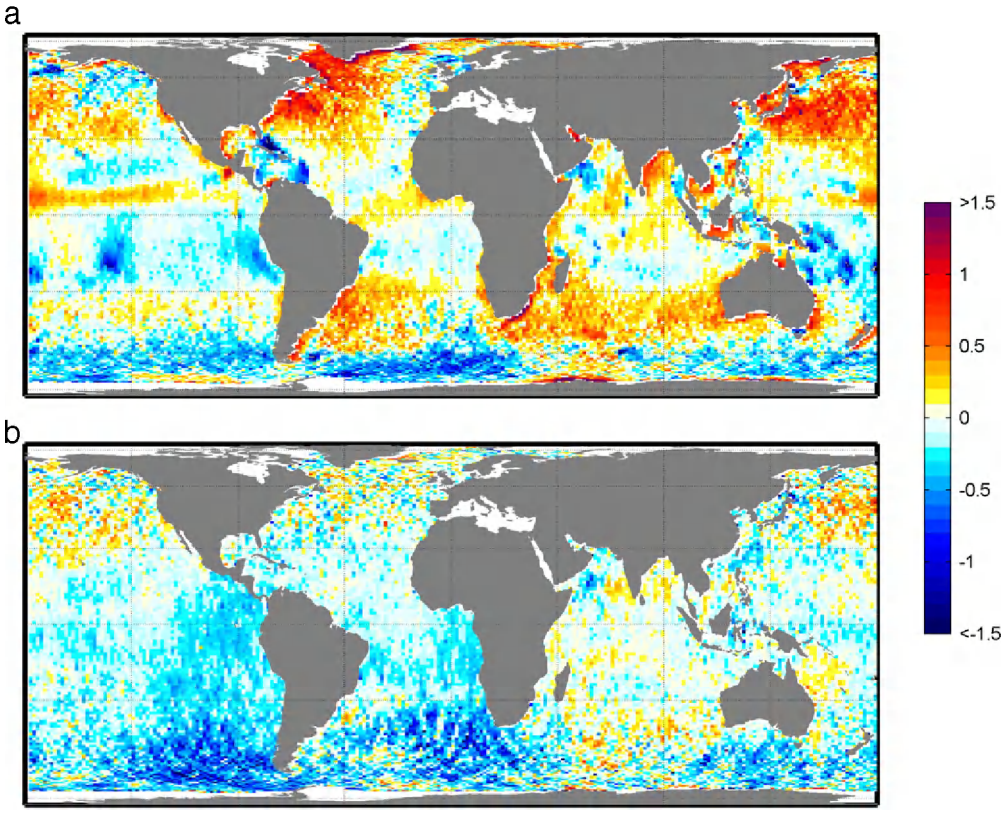


**Fig. 14.** Absolute value differences of the significant wave height 95th percentile from satellite observations (SAT) with respect to: a) NC-GOW results (SAT − NC-GOW) and b) GOW data (SAT − GOW), for the validation period from 2006 to 2008. Calibration is computed with a training set of altimeter data from 1992 to 2005.

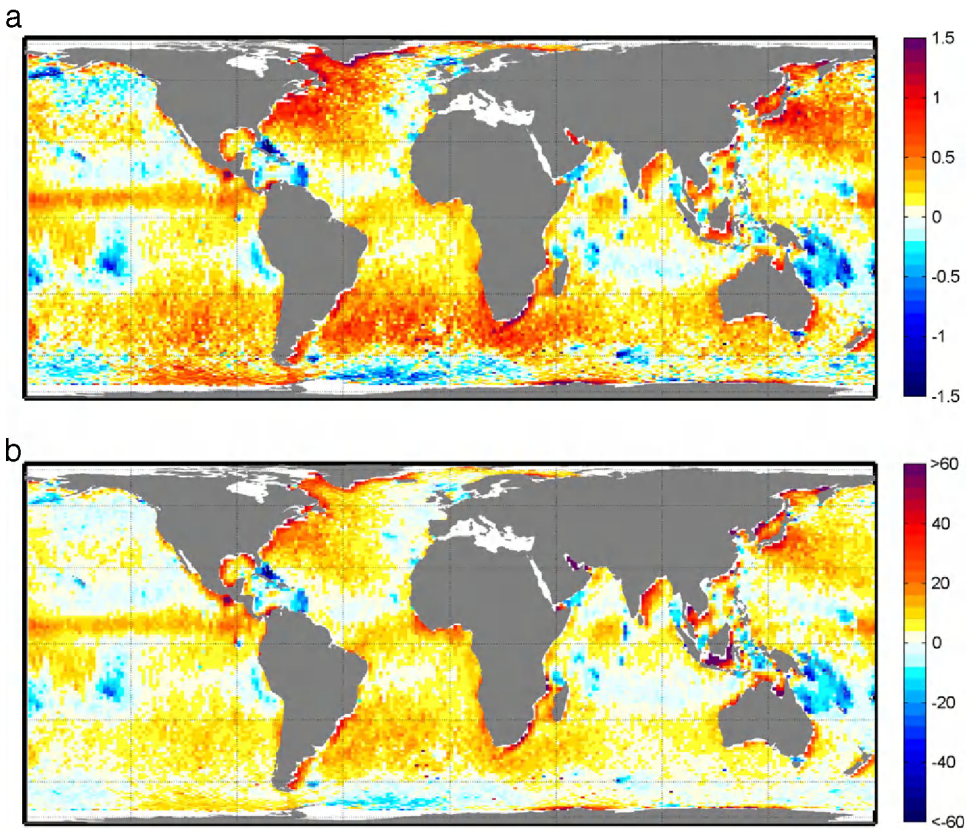


**Fig. 15.** Absolute (a; GOW — NC-GOW) and relative (b; [GOW — NC-GOW]/NC-GOW) change in the 95th percentile of significant wave height in the reanalysis data for the period from 2006 to 2008 after the calibration process. Calibration is computed with a training set of altimeter data from 1992 to 2005.

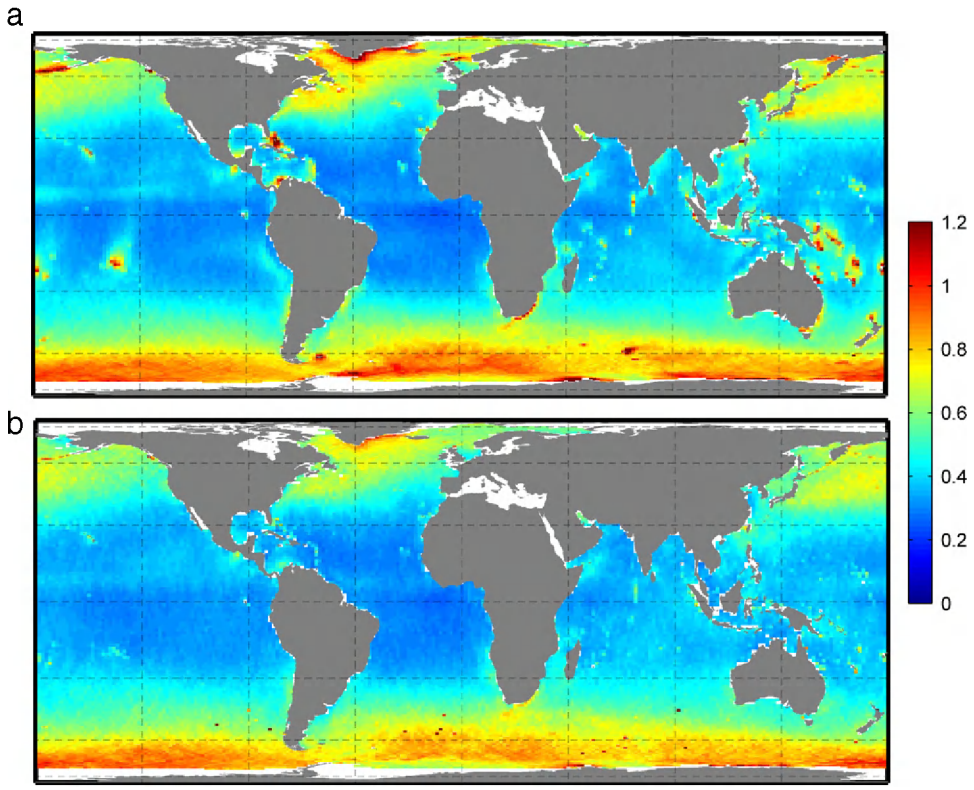


**Fig. 16.** RMSE (m) of altimetry (SAT) and the reanalysis significant wave height data, for the period from 2006 to 2008: (a) before (SAT, NC-GOW) and (b) after the calibration process (SAT, GOW). Calibration is computed with a training set of altimeter data from 1992 to 2005.

fields. For that reason, these data have been identified and removed from the analysis. The quality of the results and the corrections applied has been compared with buoy and satellite altimetry measurements. The results show a satisfactory transformation in the high quantiles distribution when necessary and no changes in areas where the initial simulated data present good agreement with respect to observations.

Additionally, a verification of the calibration method has been performed, obtaining a correction based on the altimetry data from 1992 to 2005 and judging the effect with the remaining observations. A regionally varying correction is confirmed, especially remarkable for high wave heights range and coastal regions.

After incorporating the altimeter data through the calibration process, an exhaustive validation of the results have been performed with altimeter and buoy measurements. The diagnostic statistics show a fine agreement both in the scatter data and in the statistical distribution of the wave heights indicating that the reanalysis reflects appropriately the wave characteristics identified by the satellites from 1992 to 2008.

The spatial and temporal coverage (1948 onwards) of the dataset and the results obtained in the statistical distribution for the full range of wave heights, make GOW database to be considered a long-term and consistent reanalysis, suitable for global applications in ocean wave climate as well as for coastal engineering purposes.

## Acknowledgments

The authors wish to acknowledge the NOAA, DFO and Puertos del Estado for providing its data. The altimeter data were produced and distributed by AVISO (http://www.aviso.ocanobs.com/). B. G. Reguero is indebted to the Universidad de Cantabria for the funding provided. R. Mínguez is also indebted to the Spanish Ministry MICINN for the funding provided with the "Ramon y Cajal" program. This work was partly funded by projects 'GRACCIE' (CSD2007-00067, Programa Consolider-Ingenio 2010), 'C3E' (200800050084091) and 'IMAR21' (CTM2010-15009) from the Spanish Ministry MAMRM, and 'MARUCA' (E17/08) from the Spanish Ministry MF. The study was also carried out as a part of MAREN project, partly funded by the European Regional Development Fund through the Atlantic Area Transnational Programme. The support of the European Commission through FP7.2009-1, Contract 244104 - THESEUS ("Innovative technologies for safer European coasts in a changing climate"), is also gratefully acknowledged. We also want to thank the two anonymous reviewers for their comments that contributed to the final version of the manuscript.

## References

Booij, N., Ris, R., Holthuijsen, L., 1999. A third generation wave model for coastal region, I: model description and validation. Journal of Geophysical Research 104, 769–7666.
Caires, S., Sterl, A., 2003. Validation of ocean wind and wave data using triple collocation. Journal of Geophysical Research 108, 3098. doi:10.1029/2002JC001491.
Caires, S., Sterl, A., 2005a. 100-year return value estimates for ocean wind speed and significant wave height from the era-40 data. Journal of Climate 18, 1032–1048.
Caires, S., Sterl, A., 2005b. A new non-parametric method to correct model data: application to significant wave height from the ERA-40 reanalysis. Journal of Atmospheric and Oceanic Technology 22, 443–459.
Caires, S., Sterl, A., Bidlot, J., Graham, N., Swail, V., 2004. Intercomparison of different wind-wave reanalyses. Journal of Climate 17 (10), 1893–1913 May.
Camus, P., Mendez, F., Medina, R., 2011. A hybrid efficient method to downscale wave climate to coastal areas. Coastal Engineering. doi:10.1016/j.coastaleng.2011.05.007.
Cavaleri, L., Sclavo, M., 2006. The calibration of wind and wave model data in the Mediterranean sea. Coastal Engineering 53, 613–627.
Cavaleri, L., Alves, J., Ardhuin, F., Babanin, A., Banner, M., Belibassakis, K., Benoit, M., Donelan, M., Groeneweg, J., Herbers, T., Hwang, P., Janssen, P.A.E.M., Janssen, T., Lavrenov, I.V., Magne, R., Monbaliu, J., Onorato, M., Polnikov, V., Resio, D., Rogers, W.E., Sheremet, A., McKee Smith, J., Tolman, H.L., van Vledder, G., Wolf, J., Young, I., 2007. Wave modelling. The state of the art. Progress in Oceanography 75 (4), 603–674.
Cotton, P., 1998. A feasibility study for a global satellite buoy intercalibration experiment. Southampton Oceanography Centre Resolution Consultation Report 26, Southampton Oceanography Centre. Southampton Oceanography Centre, Southampton, UK. 73.
Cox, A., Swail, V., 2001. A global wave hindcast over the period 1958–1997: validation and climate assessment. Journal of Geophysical Research 106, 2313–2329.
Dee, D.P., Uppala, S.M., Simmons, A.J., Berrisford, P., Poli, P., Kobayashi, S., Andrae, U., Balmaseda, M.A., Balsamo, G., Bauer, P., Bechtold, P., Beljaars, A.C.M., van de Berg, L., Bidlot, J., Bormann, N., Delsol, C., Dragani, R., Fuentes, M., Geer, A.J., Haimberger, L., Healy, S.B., Hersbach, H., Holm, E.V., Isaksen, L., Kallberg, P., Kohler, M., Matricardi, M., McNally, A.P., Monge-Sanz, B.M., Morcrette, J.-J., Park, B.-K., Peubey, C., de Rosnay, P., Tavolato, C., Thepaut, J.-N., Vitart, F., 2011. The era-interim reanalysis: configuration and performance of the data assimilation system. Quarterly Journal of the Royal Meteorological Society 137, 553–597.
Dodet, G., Bertin, X., Taborda, R., 2010. Wave climate variability in the north-east Atlantic ocean over the last six decades. Ocean Modelling 31 (120–131).
Feng, H., Vandermark, D., Quilfen, Y., Chapron, B., Beckley, B., 2006. Assessment of wind-forcing impact on a global wind-wave model using the TOPEX altimeter. Ocean Engineering 33 (11–12), 1431–1461 August.
Graham, N., Diaz, H., 2001. Evidence of intensification of north pacific winter cyclones since 1948. Bulletin of the American Meteorology Society 82, 1869–1893.
Hasselman, S., Hasselman, K., Janssen, P.A.E.M., Komen, G.T., Bertotti, L., Lionello, P., Guillaume, A., Cardone, V.C., Greewood, J.A., Reistad, M., Zambresky, L., Ewing, J.A., 1998. The WAM model: a third generation ocean wave prediction model. Journal of Physical Oceanography 18 (12), 1775–1810.
Hemer, M., Church, J., Hunter, J., 2010. Variability and trends in the directional wave climate of the southern hemisphere wave climate of the southern hemisphere. International Journal of Climatology 30, 475–491.
Izaguirre, C., Méndez, F.J., Menéndez, M., Losada, I.J., 2011. Global extreme wave height variability based on satellite data. Geophysical Research Letters 38 (L10607).
Kalnay, E., Kanamitsu, M., Cistler, R., Collins, W., Deaven, D., Gandin, L., Iredell, M., Saha, S., White, G., Woolen, J., Zhu, Y., Chelliah, M., Ebisuzaki, W., Higgins, W., Janowiak, J., Mo, K., Ropelewski, C., Wang, J., Leetma, A., Reynolds, R., Jenne, R., Joseph, D., 1996. The NCEP/NCAR reanalysis project. Bulletin of the American Meteorology Society 77, 437–471.
Kistler, R., Kalnay, E., Collins, W., Saha, S., White, G., Woolen, J., Chelliah, M., Ebisuzaki, W., Kanamitsu, M., Kousky, V., Dool, H., Jenne, R., Fiorino, M., 1999. The ncep/NCAR 50-year reanalysis: Monthly means cd-rom and documentation March Bulletin of the American Meteorology Society 247–268.
Komen, G., Cavaleri, L., Domelan, M., Hasselmann, K., Hasselmann, S., Janssen, P., 1994. Dynamics and modeling of ocean waves. Cambridge University Press, p. 532.
Krogstad, H.E., Barstow, S.F., 1999. Satellite wave measurements for coastal engineering applications. Coastal Engineering 37, 283–307.
Mínguez, R., Espejo, A., Tomás, A., Méndez, F.J., Losada, I.J., 2011a. Directional calibration of wave reanalysis databases using instrumental data. Journal of Atmospheric and Oceanic Technology. doi:10.1175/JTECH-D-11-00008.1.
Mínguez, R., Reguero, B.G., Luceño, A., Méndez, F.J., 2012. Regression models for outlier identification (hurricanes and typhoons) in wave hindcast databases. Journal of Atmospheric and Oceanic Technology 29, 267–285. doi:10.1175/JTECH-D-11-00059.1.
NOAA, National Geophysical Data Center, 2006. Etopo2v2 global gridded 2-minute database.
Onogi, K., Tsutsui, J., Koide, H., Sakamoto, M., Kobayashi, S., Hatsushika, H., Matsumoto, T., Yamazaki, N., Kmamahori, H., Takahashi, K., Kadokura, S., Wada, K., Kato, K., Oyama, R., Ose, T., Mannoji, N., Tairas, R., 2007. The jra-25 reanalysis. Journal of the Meteorological Society of Japan 85 (3), 369–432.
Pilar, P., Guedes Soares, S., Carretero, J., 2008. 44-year wave hindcast for the north east Atlantic European coast. Coastal Engineering 55 (11), 861–871.
Schneggenburger, C., Günther, H., Rosenthal, W., 1997. Shallow water wave modelling with nonlinear dissipation. Deutsche Hydrographische 49, 431–444.
Semedo, A., Suselj, K., Rutgersson, A., Sterl, A., 2011. A global view on the wind sea and swell climate and variability from era-40. Journal of Climate 24, 1461–1479.
Sterl, A., 2004. On the (in)homogeneity of reanalysis products. Journal of Climate 17, 3866–3873.
Sterl, A., Caires, S., 2005. Climatology, variability and extrema of ocean waves: the web-based KNMI/era-40 wave atlas. International Journal of Climatology 25, 963–997.
Sterl, A., Komen, G., Cotton, P., 1998. Fifteen years of global wave hindcasts using winds from the European centre for medium-range weather forecast reanalysis: validating the reanalyzed winds and assessing the wave climate March Journal of Geophysical Research 103 (C3), 5477–5492.
Swail, V., Cox, A., 2000. On the use of NCEP/NCAR reanalysis surface marine wind fields for a long-term north Atlantic wave hindcast. Journal of Atmospheric and Oceanic Technology 17, 532–545.
Tolman, H., 2002a. User manual and system documentation of wavewatch-iii version 2.22. September NOAA/NWS/NCEP Technical Note.
Tolman, H., 2002b. Validation of wavewatch iii version 1.15 for a global domain. NOAA/NWS/NCEP/OMB Technical Note (213), p. 33.
Tolman, H., 2009. User manual and system documentation of Wavewatch-III version 3.14. NOAA/NWS/NCEP Technical Note (276), p. 194.
Tolman, H., Chalikov, D., 1996. Source terms in a third-generation wind wave model. Journal of Physical Oceanography 26, 2497–2518.
Tolman, H., Balasubramaniyan, B., Burroughs, L., Chalikov, D., Chao, Y., Chen, H., Gerald, V., 2002. Development and implementation of wind generated ocean surface wave models at NCEP. Weather and Forecasting 17, 311–333.
Tomás, A., Méndez, F.J., Losada, I.J., 2008. A method for spatial calibration of wave hindcast data bases. Continental Shelf Research (ISSN: 0278-4343) 28, 391–398.
Uppala, S., Kallberg, P., Simmons, A., da Costa, Andrae U., Bechtold, V., Fiorino, M., Gibson, J., Haseler, J., Hernández, A., Kelly, G., 2005. The era-40 reanalysis. Quarterly Journal of the Royal Meteorological Society 131, 2961–3012.
WasaGroup, 1998. Changing waves and storms in the northeast Atlantic? Bulletin of the American Meteorology Society 79, 741–760.
Weisse, R., Von Storch, H., 2010. Marine Climate and Climate Change – Storms, Wind Waves and Storm Surges. Springer, Springer-Verlag Berlin Heidelber New York978-3-540-25316-7.
Woolf, D., Challenor, P.G., 2002. Variability and predictability of the north Atlantic wave climate. Journal of Geophysical Research 107 (C10), 3145.